Low-Wind Turbines in the Dutch Power Grid

Understanding the Effect of Low-Wind Turbines on Storage Capacity and System Costs

by

B. Vos

to obtain the degree of Master of Science in Sustainable Energy Technology
at the Delft University of Technology,
to be defended publicly on Thursday September 23, 2021 at 09:00 AM.

Student number:	4058062	
Project duration:	May 18, 2020 – September 23, 2021	
Thesis committee:	Dr. ir. M. B. Zaayer,	TU Delft, supervisor
	Prof. Dr. D. A. von Terzi	TU Delft
	Dr. ir. L. M. Ramirez Elizondo	TU Delft

An electronic version of this thesis is available at http://repository.tudelft.nl/.

TU Delft

Abstract

One of the major challenges that the world currently faces is the energy transition. The aim of most countries worldwide is to reduce their carbon footprint, in order to slow climate change. Fossil fuel powered energy generation is replaced with an increasing share of variable renewable energy sources such as wind and solar energy. Because of the inherent uncertainty and intermittency of these renewable power sources, large scale energy storage is considered inevitable in order to mitigate the mismatch between supply and demand. However, storage comes at a cost and uses precious materials, of which there might not be sufficient. Therefore, a whole range of solutions is being researched and implemented. Currently, it is not well-known what mix of which solutions will be the most technologically and economically effective.

The Low-Wind turbine is a new turbine concept, specifically designed for low wind speed conditions, combined with a low rated and cut-out wind speed. The reduced normative loads on the blades enable a re-design of several components, which ultimately results in lower costs. This new turbine concept aims to be a system-friendly turbine, by decreasing the mismatch between production and demand and thereby reducing the total amount of storage or overplanting required in the system.

This research assesses the effectiveness of the Low-Wind turbine in the Dutch energy grid, when it is predominantly powered by renewable energy sources. A power model, specifically developed for this research, simulates the power flows and optimises the seasonal storage required in order to meet the constraints. The power model is simulated for a range of installed turbines, consisting of combinations of conventional and Low-Wind turbines. This research also carries out a preliminary design off a Low-Wind turbine, based of a reference turbine, in order to determine its costs.

The result of this study show that, if the cost of the installed wind farms dominate the costs, Low-Wind turbines does not provide a cost-effective solution to minimising system costs. However, the results also show that, in a situation where total costs are dominated by storage cost, the Low-Wind turbine can provide a cost-effective alternative to conventional turbines. The results also show that, for high overplanting factors, Low-Wind turbines and conventional turbines provide a similar effect on the reduction of system costs, but at lower costs.

Preface

Before you lies the thesis 'Low-Wind Turbines in the Dutch Power Grid'. The study aims to understand the effect of Low-WInd turbines on the storage capacity and system costs. For this, a model was developed and a range of case-studies simulated and analysed, after which conclusions have been drawn.

This thesis has been written in order to obtain the Master of Science in Sustainable Energy Technologies at the Delft University of Technology. I have researched the topic and written this thesis from May 2020 to September 2021.

The project was carried out at the Delft University of Technology, where I have been supervised by Dr. ir. M.B. Zaayer. After formulating the research questions together, I started with the research. The research proved to be difficult, with a very large range of topics that needed to be addressed, but eventually the research questions could be answered. The current pandemic was extra challenging on staying motivated and achieving progress. Luckily, Dr. Zaayer was able to answer all my questions.

I would like to thank my supervisor, Dr. Zaayer, for his excellent guidance throughout this entire process. His in-depth responses to every question I had, his ability to explain all concepts simply and attention to detail has proved invaluable to me.

I would also like to thank my friends and family for their support, and especially for much needed moments of rest and relaxation throughout this demanding process.

I hope you enjoy reading this report.

B. Vos
Delft, September 2021

Contents

List of Figures

List of Tables

1

Introduction & Problem Statement

This chapter introduces the topic of this thesis and describes the steps taken to complete it. Section 1.1 presents the general topic in which this thesis belongs. Section 1.2 describes the specific focus of this thesis. Section 1.3 describes the problem analysis of this thesis. Section 1.4 describes the research questions that have been formulated. Section 1.5 presents the methods that were used to answer the research questions. Section 1.6 defines the scope of this thesis. Section 1.7 presents the report layout.

1.1. Topic & Context

"It is unequivocal that human influence has warmed the atmosphere, ocean and land. Widespread and rapid changes in the atmosphere, ocean, cryosphere and biosphere have occurred."- (IPCC, 2021).

One of the great challenges that the world currently faces is the energy transition. In order to achieve the goals set by the COP15 Paris Agreement, a substantial amount of renewable energy sources,such as solar and wind, has to be implemented into the energy systems. Although solar and wind have the potential to supply the worlds' energy demand many times over, they come with their own challenges. As these technologies depend on the weather conditions for their power generation, their output is variable and unpredictable. To solve this challenge of intermittency and unpredictability of variable renewable energy sources (VRES), this study considers the implementation of large-scale storage solutions in the future power systems to be inevitable. However, storage comes at a cost and uses precious materials, of which there might not be a sufficient amount. Therefore, other solutions can be implemented to lower the total amount of storage required, such as: demand-side management, cross-border connections or overplanting of VRES, or, potentially, new VRES concepts.

Every year the penetration of wind energy in Europe increases (Komusanac et al., 2020). In 2019, 15.4 GW of wind power was installed, resulting in a total capacity of 205 GW, as shown in Figure 1.1. Onshore installations account for 76 % of the new capacity, while 24 % is installed offshore. During 2019, 417 TW h of the generated energy came from wind power, accounting for 15 % of Europe's total electricity consumption.

The yearly increase in installed capacity is a good trend overall, as it reduces the amount of fossil fuels needed to meet Europe's electricity demand. However, during periods where wind speed lower than about 11 $\mathrm{m\,s^{-1}}$, the actual maximum amount of wind power that is available at any moment in the future is unpredictable, since it is proportional to the wind speed cubed at that time, which in turn relates to the weather. Moments of high wind-speeds can result in an excess of wind energy, resulting in low, and sometimes even negative electricity prices (Amelang et al., 2018). Negative energy prices can occur when high and inflexible power generation and low electricity demand appear at the same time. In hours of high (predicted) renewable energy power supply, producers offer their electricity for prices below zero. Wind and solar plants are not reliant on fuel for their production and therefore they can offer their power for the lowest price and are dispatched first.

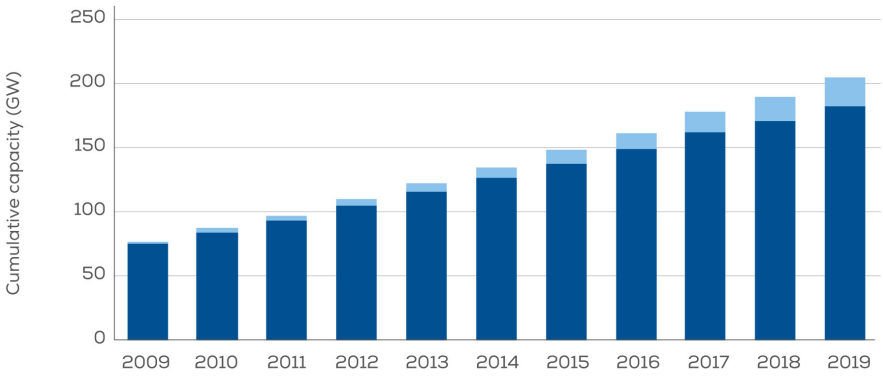

	2009	2010	2011	2012	2013	2014	2015	2016	2017	2018	2019
Offshore	2	3	4	5	7	8	11	13	16	18	22
Onshore	75	84	93	105	115	127	137	149	162	171	183
Total	**77**	**87**	**97**	**110**	**122**	**135**	**148**	**162**	**178**	**189**	**205**

Figure 1.1: Total installed wind power capacity in europe from 2009 to 2019 (Komusanac et al., 2020)

It is very rare to have moments in time when the total demand is exactly met by renewable generation. At 6:00 AM on January 1^{st}, 2018 was the first time ever that approximately 100 percent of Germany's demand was met by renewable generation (Amelang, 2018). Moreover, while there have been moments before when the total demand can be satisfied by renewable energy alone, conventional power plants will still be running for several reasons. These reasons can be either technical or economical. A technical reason for a conventional plant to keep running may be that the plant is unable to ramp-up or down their production fast enough. An economical reason may be that the shutting down and starting back up is too expensive. The plant may also need to keep operating in order to provide heat to a district heating network or provide power in the balancing market.

Another problem that arises in power systems as the share of VRES increases is the loss of system inertia (Ulbig et al., 2014). In a traditional power system, the generation of electricity is supplied by fully dispatch-able and controllable plants and involves rotating synchronous generators. These generators add rotational energy to the system through the kinetic energy stored in their flywheels/mass. Due to electro-mechanical coupling the generator's mass can supply or absorb energy from the grid in case of a frequency deviation δf. The grid frequency has to be kept within a certain range for the stable operation of the power system. Deviations from the nominal frequency f_0 have to be kept small to reduce damage in synchronous machines. For even larger frequency deviations load shedding can occur.

Since wind turbines and Photo-voltaic (PV) units are connected to the grid through an inverter, they are essentially decoupled from the grid and do not detect deviations in the system (Ulbig et al., 2014). The inverter is designed in order to maximise the power output of the VRES plant at any given time. As VRES penetration increases, the system's dynamics change. In large power systems the rotational inertia becomes location and time-variant, depending on the amount of VRES-power being inserted in a certain area at a certain moment. Large-scale integration of VRES moves the power system towards an inverter dominated scenario, as shown in Figure 1.2. Reduced rotational inertia results in amplified frequency dynamics and in turn larger frequency deviations.

The future Dutch energy system has to be a lot more flexible in order to cope with the high penetration of VRES. A certain security of supply is expected by all the users of the grid and this has to stay stable. The electrification of other sectors, such as transport and industry, puts even more strain on the electricity network. These future challenges can be countered by a combinations of solutions, both technical and nontechnical (Madsen et al., 2019), such as:

- A more flexible power system;
- Smart grids;

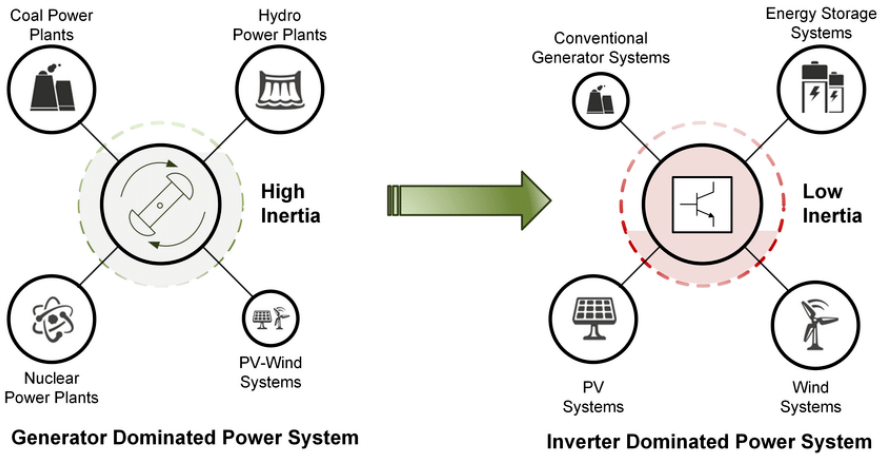

Figure 1.2: Schematic representation of trend towards power systems with low system inertia. (Tamrakar et al., 2017)

- Demand-side management
- Batteries and other storage solutions;
- Stronger cross-border grid connections;
- Increased total capacity of Variable Renewable Energy Sources (VRES);
- Low wind speed turbines (explained below).

1.2. Focus

Historically, conventional wind turbines are designed to reach their rated power at wind speed around 11 to 13 $\mathrm{m\,s^{-1}}$. Because a feed-in tariff (FIT) was paid for every produced kW h, wind farms were insensitive to the actual wholesale energy prices, which reflect the balance between supply and demand (May, 2017). The main goal for a wind turbine design was to maximise the amount of produced energy for minimal costs. This gave investors certainty for their return of investment but did not create incentive to install system-friendly wind turbines. For a wind turbine, system-friendly designs aim at improving overall system integration, rather than only minimising energy production cost.

A system-friendly solution might be a turbine with lower specific power (SP). The SP of a wind turbines is defined as its rated power divided by its rotor diameter and is expressed in $\mathrm{W\,m^{-2}}$. The reduced SP can be achieved by combining a relatively large rotor with a small generator, compared to conventional turbines. This results in turbines that can effectively produce energy at low wind speeds. These so-called low wind speed turbines (LWST) produce more power at low wind speeds, have less volatile energy production and increased annual full load hours (AFLH)(Dalla Riva et al., 2017).

This study focuses on a potential new VRES concept, namely the Low-Wind turbine concept. This turbine concept is specifically designed for low wind situations, combined with a low rated and cut-out wind speed. The reduction in rated wind speed reduces the loads on the turbine, which in turn reduces the amount of material required and therefore the cost of several components, when compared to conventional turbines of similar size. These turbines have a power curve that is shifted to the left, reaching rated power at low wind speeds, and a cut-out wind speed at or around the point where conventional turbines reach rated wind speeds, as shown in Figure 1.3. The ”Conventional” power curve shows a typical power curve of turbines that are currently installed, while the ”LowWind” curve shows the power curve of the new turbine concept.

Because of their altered power curve compared to conventional turbines, they compete less with other conventional wind turbines in the energy market, as they generally produce significant energy during different time periods. During high wind speeds, when conventional turbines are operating at rated power, the Low-Wind turbines are shut off. The Low-Wind turbine concept aims to be a system-friendly turbine by decreasing the mismatch between production and demand and thereby reducing the total amount of storage or over-planting needed in the system. this study investigates the effect of the implementation of Low-Wind turbines in the Dutch power system.

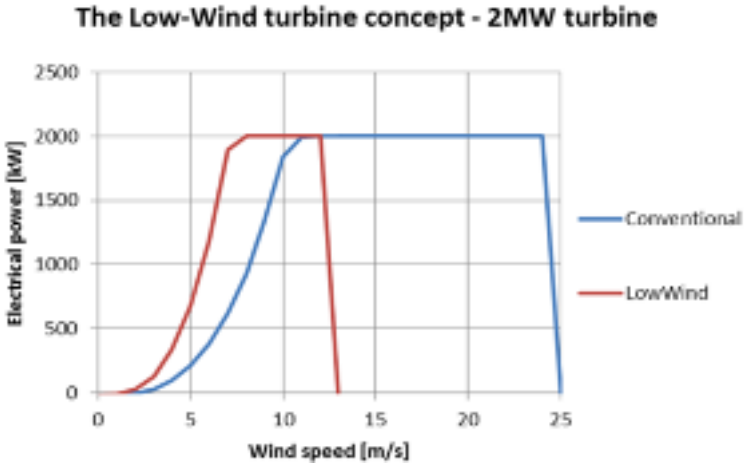

Figure 1.3: graph showing power-curves of a conventional and a low-wind turbine (Madsen et al., 2019)

1.3. Problem Analysis

Wind turbines have historically been designed to produce rated power at high wind speeds, mainly due to feed-in tariffs. However, as the penetration of wind turbines and other VRES increases in order to meet the goals set in the COP15 Paris agreement, the intermittency and uncertainty of these VRES pose challenges that need to be overcome. Solutions such as a more flexible power system, smart grids, storage, stronger cross-border links, an increased total capacity of VRES and Low-wind turbines all have to be taken into consideration and their effectiveness researched. A combination of these solutions, if not all solutions, will have to be implemented in order to create the sustainable energy system of the future.

Currently, it is not well-known what mix of solutions will be the most technologically and economically effective. For this study it is assumed that storage will play a major role in the future energy system, to mitigate the effects of intermittency and uncertainty of supply. This study will focus especially on the technical and economic effects the Low-wind turbine concept has on the required amount of seasonal storage and the combined cost of storage and offshore wind farms. Since such a Low-wind turbine are not yet in use, there currently is little knowledge available about technical and economic viability of such a turbine. This study will also carry out a preliminary design of such a turbine in order to create insight in the technical and economic viability. With this information, this study draws conclusions about the effectiveness of the Low-wind turbine concept. Given that these turbines can be produced cost-effectively, they may be able to cost-effectively reduce the amount of storage capacity needed to create an energy system running predominantly on VRES.

1.4. Research Questions

In this study of the Dutch power system, the main objective is to understand the effect of the new Low-Wind turbine concept on the required storage capacity and costs of the energy system. Sub-questions used to achieve his objective are listed below:

- What will be the cost of a Low-Wind turbine?
- What is the effect of implementing Low-Wind turbines in the Dutch power system on the required seasonal storage capacity?
- What is the effect of different storage technologies on the required seasonal storage capacity?
- What is the effect of implementing Low-Wind turbines in the Dutch power system on the system costs?
- What is the effect of different storage technologies on the system costs?
- how sensitive are these effects to the cost of the Low-Wind turbines?
- How sensitive are these effects to the cost of the storage technologies?

1.5. Methodology

This section briefly describes the activities done to answer the research questions. These activities are:

1. Develop the power system model for the Dutch power system, containing models to simulate wind and PV power, demand, storage and cross-border connections;
2. Develop Low-Wind turbine scaling and cost model;
3. Determine optimisation criteria and develop an algorithm to optimise the required storage capacity for a certain amount of installed offshore turbines and constant onshore VRES;
4. Develop cost calculation method;
5. Obtain historic demand time series for the Dutch energy system;
6. Obtain historic meteorological data for the same year as the demand, in order to have correlation between demand and weather conditions;
7. Obtain cost figures for power system components;
8. Collect and analyse results of initial simulations;
9. Develop and perform sensitivity analysis, discuss results and generalise results.

1.6. Scope

In this section, the scope of the thesis is defined as:

- This research is limited to the Dutch power system;
- This research incorporates geospatial variation in VRES power output;
- All simulations in this research contain a fixed amount of onshore Photovoltaic power generation;
- All simulations in this research contain a fixed amount of onshore wind power generation;
- This research will only focus on the design of an offshore Low-Wind turbine;
- This research will **not** focus on optimal wind farm layout;
- This research uses historical data to model the demand of the Dutch power system;
- The model only simulates power flows, and does not deal with active and reactive power;
- Grid congestion is not considered an issue in this research;
- The Low-Wind turbine is designed by applying scaling relations to a reference turbine;
- The models developed during this research are not validated against other models;

1.7. Readers Guide

This section describes the layout of the report. Chapter 2 describes the working principles of the power system model that was developed for and during this thesis. The chapter starts with a flowchart and general overview of the power system model, after which the physical equations used to model the individual components are described. Then, the storage optimisation algorithm is presented, after which the model and optimisation algorithm are verified to be working properly. Finally, the cost calculation method is presented. Chapter 3 describes the scaling and cost model that is developed to design the Low-Wind turbine and determine its cost. A flowchart is used to visualise the different components of the turbine scaling model. After this, the rationale behind the scaling philosophy are described. Then, the scaling and cost rules are described per considered turbine component. Finally, the equation for the cost of the newly designed Low-Wind turbine is presented. Chapter 4 presents the inputs used in the simulations. First, the two reference turbines used in this study are presented. The

model uses an onshore turbine for the onshore wind parks. The offshore turbine serves two purposes: it serves as the conventional offshore turbine and as a the reference turbine which the Low-Wind turbine is based off of. Then, the parameters for the onshore and offshore wind farms are presented. Then, the parameters for the solar farms are described. Lastly, the parameters are given for the different storage technologies that have been simulated. Three different storage technologies have been simulated, of which their characteristics and costs are presented. Chapter 5 presents and discusses the initial results from the model, as well as the sensitivity analysis. The results show the effect of the Low-Wind turbine has on the required storage capacity and costs. The sensitivity analysis shows the effect of changing costs of the Low-Wind turbine and the storage technologies. Combining the results of the initial simulation and the sensitivity analysis, general conclusions about the effectiveness of Low-Wind turbines are drawn. Chapter 6 concludes this thesis by answering the research questions and giving recommendations for future research that can expand upon this thesis.

2

Power System: Model Description

This chapter describes the working principles behind the different modules in the electric grid model. Section 2.1 presents and describes the complete model of this thesis using a flowchart. Section 2.2 further details the main components of the power flow model. Section 2.3 presents the implementation of wind power in the model. Section 2.4 describes the working principles of solar power within the power flow model. Section 2.5 describes the modelling of the energy storage. Section 2.6 describes the data used for the Dutch energy demand. Section 2.7 explains the optimisations algorithm that was developed to optimise the storage capacity. Section 2.8 describes the calculation of the yearly total system cost. Section 2.9 presents and discusses the verfication of the power model and optimisations constraints.

2.1. Flowchart

The power model consists of generation, storage and consumption. The electricity system is modelled to simulate power flows and supply and demand matching on an hourly timescale. Short term power fluctuations, AC power factor correction,grid stability and grid congestion are not modelled. Figure 2.1 gives a graphical representation of the model. The flowchart can be read from left to right. The orange slanted blocks indicate model inputs, the blue squares indicate the different model components and the green slanted blocks indicate model outputs. The power model runs for a set amount of conventional, Low-Wind offshore turbines and storage capacity. These offshore turbines are distributed over the offshore parks such that each parks is filled to the same percentage of its maximum capacity. The power flow model simulates the power flow between generation, load, storage, import and export. The outputs of this model are timeseries for the different parameters within the model, such as import, export, state of charge, etc. Based on the values of these timeseries, the storage optimiser uses a root-finding algorithm to determine the amount of storage needed to satisfy the constraints. The optimisation is explained in more detail in Section 2.7. The wind farm and storage cost model determine the CAPEX and OPEX for the installed wind turbines and storage, respectively.

2.2. Power Flow Model Overview

In Figure 2.2 a schematic representation of the power flow model is shown. This model consists of 5 components: wind power, solar power, load, storage and import/export to other countries. Each wind- and solar farm has a different geographical location, and the model selects the nearest available dataset from the meteorological hindcast data. Using the wind speed and irradiation at the specific location, the model calculates power generation for every time step. The onshore wind and solar generation are grouped into a single geographical location per province. The offshore wind farms also us a single location per farm, as to not accidentally place one of the types at a more favourable location, which could skew the results. The load is modelled using historical data, which represents the total electric energy demand of The Netherlands (ENTSO-E, 2021). For a given amount of onshore turbines and PV-area are installed for every province, explained in Section 2.3.9 and Section 2.4.2. Specifics of the simulations and their respective inputs are explained in Chapter 4.

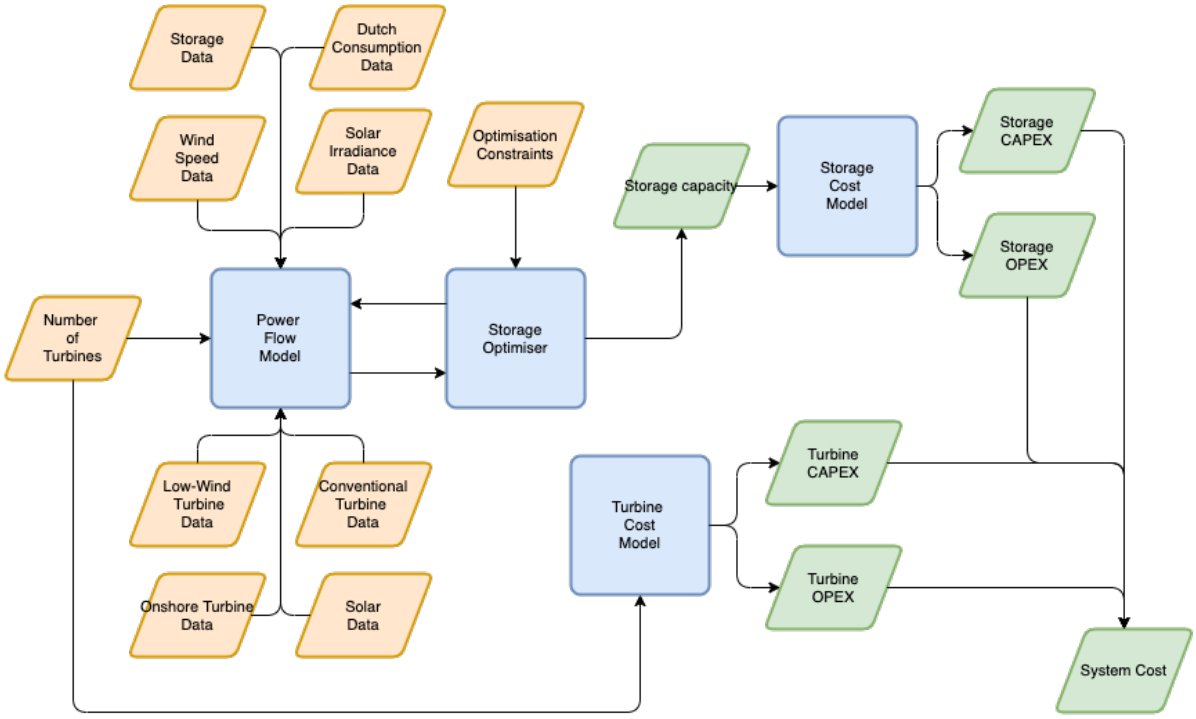

Figure 2.1: Conceptual overview of the model used in this thesis

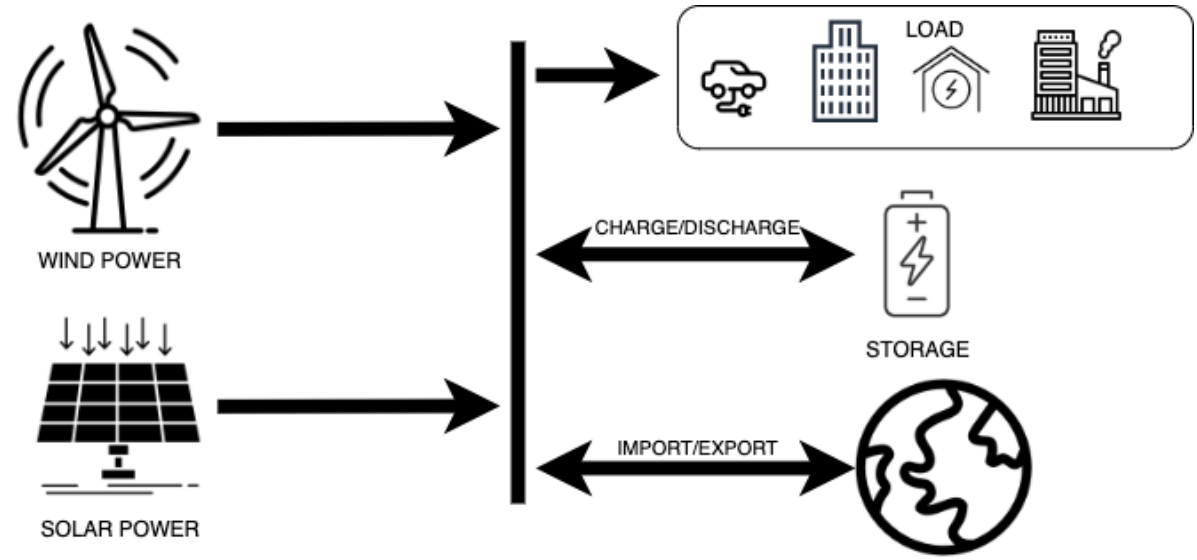

Figure 2.2: Schematic representation of the power flow model of the dutch grid

2.3. Wind Power

This section describes the implementation of wind power in the model. The redesign of the Low-Wind turbine and calculation of its cost is more elaborate, and therefore explained in Chapter 3. Each simulation, explained in Chapter 4, consist of the same amount of onshore turbines and PV farms, and a variable amount of offshore turbines. The Low-Wind turbine will only be placed in the offshore locations. The fixed onshore capacity is divided over the different provinces, to create location dependent power generation. Section 2.3.1 describes how the model calculates the generated power for a wind turbine. Section 2.3.2 describes the wind speed data. Section 2.3.3 explains the turbine spacing and thereby the land use per turbine. Section 2.3.4 states loss factors for the wind farms. Section 2.3.5 describes the locations and area available for offshore wind turbines. Section 2.3.6 states the costs of the components

of an offshore wind farm. Section 2.3.7 states the installation costs of the different offshore wind farm components. Section 2.3.8 describes the maintenance, operations and decommissioning costs of a wind farm. Section 2.3.9 describes the locations and area available for onshore wind turbines. Section 2.3.10 describes the reason why the costs of the onshore wind farms are ommitted from this study.

2.3.1. Turbine Power Generation

The power generated by a single wind turbine is modeled using the power curve of the turbine. Because of the large time-step used in the model, turbulent fluctuations of the wind speed and direction are assumed to even out, and the average wind speed per hour is used. The equation for the power of a turbine is stated in Equation (2.1):

$$P_{turbine}(t) = \begin{cases} 0 & \text{For } V_{cut-in} > V_{hh}(t) > V_{cut-out} \\ \frac{1}{2} \cdot \eta_{turbine} \cdot c_P \cdot \rho_{air} \cdot A_{rotor} \cdot V(t)_{hh}^3 & \text{For } V_{cut-in} < V_{hh}(t) < V_{rated} \\ P_{rated} & \text{For } V_{rated} < V_{hh}(t) < V_{cut-out} \end{cases} \tag{2.1}$$

Where $P_{turbine}(t)$ is the turbine power output at time t, $\eta_{turbine}$ is the turbine efficiency, c_P is the design coefficient of performance, ρ_{air} is the density of air, A_{rotor} is the rotor diameter, $V(t)_{hh}^3$ is the wind speed at hub height at time t, V_{cut-in} and $V_{cut-out}$ are the cut-in and cut-out wind speeds, respectively. The wind speed at hub height is calculated by applying the power-law to the measured windspeed. The power law is stated in Equation (2.2) (Manwell et al., 2002).

$$V(h) = V(h_{ref}) \cdot \left(\frac{h}{h_{ref}} \right)^{\alpha} \tag{2.2}$$

Where $V(h_{ref})$ is the known wind speed at reference height, h is the height where we want to know the wind speed, h_{ref} is the reference height and α is the power law exponent. For α two values can be used, depending on the location of the wind turbine.

Table 2.1: Overview of α-values for different wind turbine locations (M. Zaayer et al., 2018)

Wind Turbine Location	**Typical α-value**
Land Based	0.143
Off-Shore	0.11

2.3.2. Wind Speed Data

The wind speed data used in this model comes from the European Center for Medium Range Weather Forecasts (ECMWF). The ECMWF uses forecast models and historic data to create global data sets of the atmosphere, land surface and oceans. The model uses ERA5 hindcast data(Hersbach et al., 2018) for the calculation of the wind power generation at every timestep. Using historic data and atmospheric models they produce a grid of estimates of atmospheric conditions, essentially filling in the spatial gaps between measurement locations. The dataset used in the model consists of the reanalysis data for 2019. 2019 is chosen as this is the same year as the load data, so there is correlation between the load and weather conditions. The data has a temporal resolution of 1 hour, and a spatial resolution of 0.25° × 0.25°. A time-step of 1 hour is deemed sufficient to research the effect of the Low-Wind Turbine on seasonal storage.

2.3.3. Turbine Area Use

The amount of turbines that can be installed in a given wind farm location is determined by the total area available and spacing of the turbines. For ease of calculations, the turbines are assumed to be placed in a rectangular pattern with sides of length $m \cdot D$ and $n \cdot D$ meters, as shown in Figure 2.3. In the figure side $m \cdot D$ is square, while $n \cdot D$ is parallel to the prevailing cross wind direction. In this study the wind farms will all have a uniform spacing of $m = 5$ and $n = 10$, as this reduces the array losses of wind farm (Manwell et al., 2002).

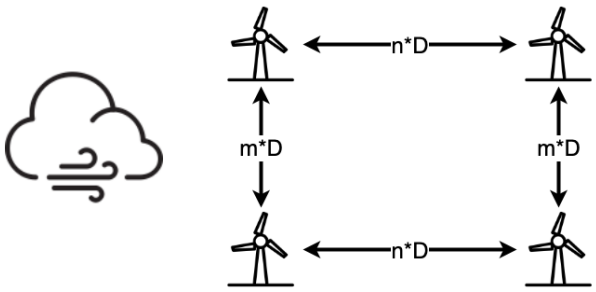

Figure 2.3: Schematic representation of turbine spacing

This results in the simple Equation (2.3) for calculation of the area-use per turbine $A_{turbine}$, with D_{rotor} the rotor diameter and m and n being values for the amount of rotor diameters between turbines. The amount of turbines in a wind farm is then easily calculated by dividing the total area available by the area-use per turbine.

$$A_{turbine} = m \cdot n \cdot D_{rotor}^2 \tag{2.3}$$

2.3.4. Wind Farm Losses

In order to make the wind farm model a more realistic representation of reality, the power model implements wind farm losses. This thesis takes the following losses into account: wake losses, transportation losses, and availability of the wind turbines in the wind farm. Wake losses are a result of decreased wind speed and increased turbulence due to energy extraction by the upwind turbines. Transportation losses are a result of electrical losses in the export cables. All wind farms will use an AC grid connection. Availability of the wind turbines in the wind parks is not 100 %, as turbines will be unavailable for production due to maintenance or failure. The effect of these three losses on the wind farm power output can be calculated using Equation (2.4):

$$P_{farm}(t) = P_{turbine}(t) \cdot N_{turbs,farm} \cdot \eta_{wake} \cdot (\eta_{transport} \cdot L_{cable,transport}) \cdot \eta_{availability} \tag{2.4}$$

where $P_{turbine}(t)$ is the power output of the undisturbed turbines, $N_{turbs,farm}$ is the number of turbines in the wind farm and η_{wake}, $\eta_{transport}$, $\eta_{availability}$ are the efficiencies due to wake losses, transport losses and turbine availability, respectively. Based on a wind farms geographical location, the length of the wind farm export cable $L_{cable,transport}$ is determined by taking the shortest straight path to either IJmuiden, Borssele or Eemshaven.

2.3.5. Offshore: Installed Capacity

Figure 2.4 shows a map of the area of interest for this study. Within this offshore area, the Exclusive Economic Zone (EEZ) of the Netherlands, the Dutch government selected designated areas for the exploitation of offshore wind. This study uses these areas in the powermodel, filling the areas with conventional and Low-Wind wind turbines. Each wind farm gets a geographic coordinate for which the nearest hindcast data is found. The Dogger Bank, which is in the top left corner of the EEZ is also considered. For a certain simulation, the amount of turbines are divided over each park such that all parks are filled for an equal percentage of their maximum.

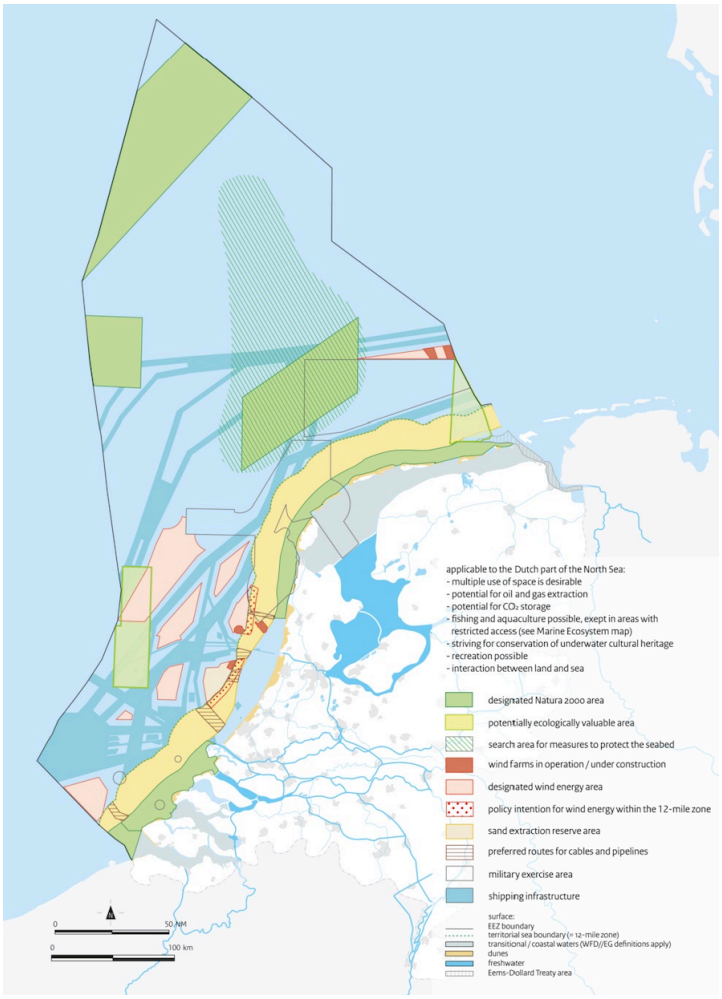

Figure 2.4: Map of Dutch Exclusive Economic Zone indicating designated areas (UNESCO, 2021)

2.3.6. Offshore: Components Costs

A wind farm consists of several other major components, besides the actual wind turbines. These components are called the Balance of Plant (BOP). The BOP consists of the following components: array and export cables, Offshore substations, onshore substations and an operations base. The cost figures of the different components used in the model are described in Section 4.3.4.

2.3.7. Offshore: Installation Cost

Beside the cost of the components of the wind farm, they will also have to be installed. The installation costs of an offshore wind farm considered in this study are: Foundations, substations, offshore cable installation, export cable installation, turbine installation. Other costs which are considered ass well are logistic costs and other costs, such as insurance and contingency. The cost figures used for the different installation costs are described in Section 4.3.5.

2.3.8. Offshore: Maintenance, Operations and Decommissioning Costs

The Operations and Maintenance (O&M) costs of a wind farm are assumed to be constant and independent of turbine rated power. The O&M consist of tasks such as personnel training, health and safety, control and operation of the wind turbines and BOP. Maintenance tasks are performed to keep the wind farms operational during their lifespan and consists of planned maintenance and response to unforeseen faults. Both the operations and maintenance cost figure occur on a yearly basis. The cost figures used for the O&M costs are described in Section 4.3.6.

2.3.9. Onshore: Installed Capacity

The Dutch power grid modelled in this thesis will be partially powered by onshore wind turbines. The amount of onshore turbines is a fixed amount of installed power for every simulation. The installed capacity for every province will be satisfied by installing land-based reference turbines until that capacity is satisfied. For simplicity, a single wind farm is created for each province. The desired installed capacity per province is described in Section 4.3.2.

2.3.10. Onshore: Costs

The cost of the onshore wind farms in this study are not calculated. Since the onshore wind farms are kept constant for all simulations, these will just add a constant cost value. This unchanging cost figure is not of interest to the study, so it is therefore omitted.

2.4. Solar Power

This section describes the implementation of solar power in the model. For each simulation, described in Chapter 4, the solar power partially powers the Dutch energy grid. The model uses a fixed installed solar capacity for all simulations. Section 2.4.1 describes the working principles of the solar power calculations Section 2.4.2 describes the method for the sizing of the solar installed capacity. Section 2.4.3 gives an explanation for the fact that the cost of solar is not importance to this thesis.

2.4.1. Solar Power Generation

For the calculation of the power output of a PV array, the amount of radiation, irradiance for short, on the PV surface has to be determined. The equations used to model the solar irradiance on a pv model are taken from (Smets et al., 2016). Figure 2.5 gives a schematic representation of the direct, diffuse and reflected component of solar radiation incident on a tilted PV surface.

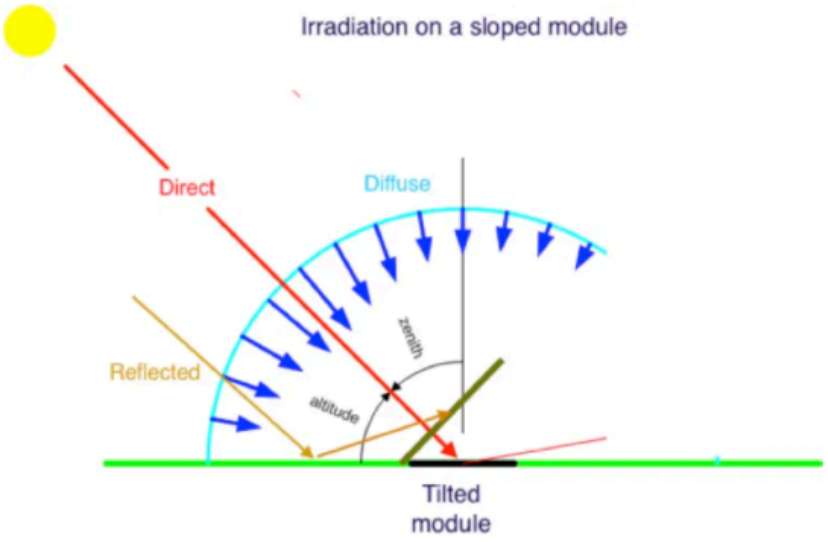

Figure 2.5: Schematic representation of the different components of solar radiation incident on a PV surface (Ecosmartsun, 2021)

To calculate the irradiance on a PV surface at a given location and time we need to know the amount of solar radiation coming from the sky, the position of the sun and the orientation of the PV surface.

The model uses ERA5 hindcast data(Hersbach et al., 2018) for the calculation of the solar power generation at every timestep. The two irradiation variables used in this thesis are ”Surface solar radiation downwards” and ”Total sky direct solar radiation at surface”, where the first represents the Global Horizontal Irradiation (GHI), and the latter represents the Direct Normal Irradiance (DNI). The total irradiance on a PV module $G_M(t)$ can be calculated using Equation (2.5),

$$G_M(t) = G_M^{direct}(t) + G_M^{diffuse}(t) + G_M^{ground}(t) \tag{2.5}$$

where G_M^{direct} is the direct component from the sun, $G_M^{diffuse}$ is the diffuse component coming from the rest of the sky and G_M^{ground} is the reflected radiation from the ground. These components can be calculated using Equations (2.6) to (2.8),

$$G_M^{direct}(t) = DNI(t) \cdot \cos(\gamma(t)) \tag{2.6}$$

$$G_M^{diffuse}(t) = GHI(t) \cdot SVF \tag{2.7}$$

$$G_M^{ground}(t) = GHI(t) \cdot \alpha_{ground} \cdot (1 - SVF) \tag{2.8}$$

where $\cos(\gamma(t))$ is the cosine of the angle between the normal vector of the tilted PV module and the direct solar beam, SVF is the Sky View Factor and α_{ground} is the ground albedo. After calculation of the irradiance on a module, the AC power at each time-step $P_{AC}(t)$ is calculated using Equation (2.9),

$$P_{AC}(t) = A_M \cdot G_M(t) \cdot \eta_{PV} \tag{2.9}$$

where A_M is the module surface area and η_{PV} is the total PV system efficiency. In reality, total PV system efficiency comprises a lot of different components and is a function of temperature and irradiation. However, the modelling of these effects results in lengthy calculations.

2.4.2. Solar: Installed Capacity

For the total solar installed capacity a different approach is developed, as there are no clear goals for the amount of installed capacity by either 2030, or 2050. Instead, it is derived using the data available for the onshore wind turbines, and the goal set by the Dutch government, to have a total annual energy production on land of at least 35 TW h by 2030 (Ministerie van Economische zaken en Klimaat, 2019). Since the area available for onshore wind turbines is fixed, as stated in Section 2.3.9, the yearly production of these wind turbine is calculated using the model. This yearly production can then be subtracted from the 35 TW h goal to determine the production needed from solar energy. The total surface area of solar panels needed to satisfy the production goal is found using a root-finding algorithm. for this, and the rest of the optimisation problems in this thesis, Brent's method is used for the root finding algorithm. The function that is used to determine the required solar panel is stated in Equation (2.10):

$$f(x) = E_{tot,onshore} - E_{tot,wind} - E_{tot,solar}(x) \tag{2.10}$$

Where $E_{tot,onshore}$ is the desired annual onshore energy production, $E_{tot,wind}$ is the total annual onshore wind energy production and $E_{tot,solar}(x)$ is the total annual solar energy production for a certain solar area x.

All PV arrays in the model are south facing with a tilt angle of 35°, and a row distance of 9 m. This orientation produces the largest annual energy yield, while the row spacing ensures that shading of the panels does not occur.

2.4.3. Solar: Components and maintenance Costs

The cost of the PV installation and maintenance are not calculated in this study. The different scenarios for which the model is run all use the same amount of solar power. Essentially, the modelled PV installation is constant for all scenarios. Therefore, it is not deemed necessary to calculate the costs of this pv installation, as these will be the same for all scenarios.

2.5. Energy Storage

This section describes the modelling used for the storage in the system. Section 2.5.1 describes the characteristics that have been used to model the storage technologies. Section 2.5.2 describe the storage charging and discharging logic. The different types of storage that have been analysed in this study are presented in Section 4.5.

2.5.1. Storage Characteristics

This study focuses on the effect of Low-Wind Turbines on the amount of seasonal storage and ultimately the cost-effectiveness of this new turbine concept. The power model models all storage technologies in

the same way, based on 4 characteristics: Capacity, efficiency, maximum discharge rate and maximum depth of discharge (DoD) The maximum charge and discharge rates of the storage capacities are all limited to 20 % of their total capacity per time step.

2.5.2. Charging and Discharging Logic

The storage in the system is used to mitigate the mismatch between the load and supply as much as possible. The working principle of the storage model is shown in the flowchart in Figure 2.6. The storage technologies are all insensitive to market incentives. The maximum amount that the storage can store for each timestep is bounded by its maximum charge-rate and its maximum allowable state of charge (SOC). The minimum amount that can be stored for each time step is bounded by its maximum discharge-rate and it minimum allowable SOC. All energy that can not be stored is exported to neighbouring countries or curtailed. All energy that can not be supplied by storage is imported from neighbouring countries. Efficiencies are applied twice, both when charging and discharging.

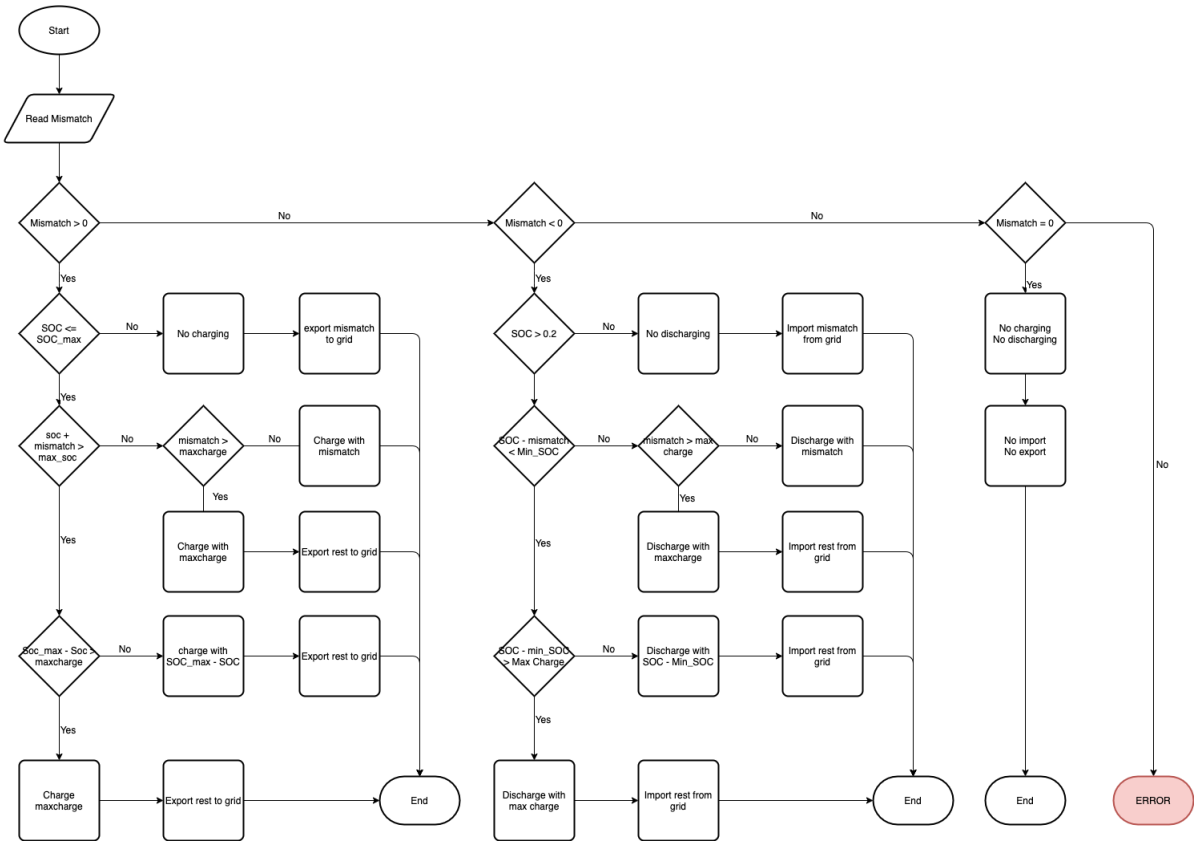

Figure 2.6: Flowchart showing the battery model charge and discharge logic

2.6. Dutch Energy Demand

The energy demand in 2050 is modelled using an existing historic dataset for the entirety of The Netherlands. This data is made publicly available by ENTSO-E, on their transparency platform (ENTSO-E, 2021). This is a simplistic approach to model the future energy demand of The Netherlands. The energy demand in 2050 will most likely have a different pattern compared to the one we see today. Advancements in efficiencies of electric devices decrease the total yearly amount of energy required. Market mechanisms such as demand-side management, where demand shifts to a period where there is sufficient generation, can change the shape of the daily load curve. Furthermore, the increasing population of The Netherlands increases the total amount of energy. The electrification of previously fossil-fuel powered sectors puts another strain on the Dutch electric grid. The effects that the phenomena described above have on the shape of load profile is beyond the scope of this thesis.

2.7. Storage Optimisation

This section explains how the sizing of the storage within the system is done for each simulation. The goal of the system sizing is to determine the amount of storage needed for a certain amount of conventional and Low-Wind turbines, in order to determine the effect of implementing the Low-Wind turbines on the total amount of storage capacity required. The power flow model consists of the following components: generation, demand, storage and import/export to neighbouring countries. The generation and storage components have to be sized correctly, such that the energy system functions properly, at minimal costs. As already discussed in the previous section, the onshore generation in the form of solar and wind is fixed for all scenarios. Demand can not be changed and has to be satisfied at every time-step, as it is not desirable to be without power. Import and export of energy act as a safety net, ensuring that demand can still be satisfied in situations where the Dutch generation and storage fail to do so.

The system is sized by formulating constraints for the import and export and calculating the minimum amount of storage needed that satisfies these constraints. The constraints on the system are stated in Equations (2.11b) to (2.11i):

$$\min_x f(x) = \text{amount of storage} \tag{2.11a}$$

$$\text{s.t.:} \quad P_{storage}(t) + P_{VRES}(t) + P_{import}(t) = P_{demand}(t) \quad \forall t \tag{2.11b}$$

$$E_{onshore,annual} = 35\,\text{TW h} \tag{2.11c}$$

$$P_{export}(t) \cdot P_{import}(t) = 0 \quad \forall t \tag{2.11d}$$

$$SOC(t=0) \leq SOC(t=T_{end}) \tag{2.11e}$$

$$E_{produced,annual} \geq 90\% \cdot E_{demand,annual} \tag{2.11f}$$

$$E_{import,annual} \leq 10\% \cdot E_{demand,anual} \tag{2.11g}$$

$$E_{export,annual} \leq 10\% \cdot E_{demand,anual} \tag{2.11h}$$

$$P_{import}(t) \leq \left(90\% \cdot \frac{P_{VRES}(t)}{P_{VRES,total}} + 10\%\right) \cdot P_{import,max} \quad \forall t \tag{2.11i}$$

$$P_{export}(t) \leq \left(-90\% \cdot \frac{P_{VRES}(t)}{P_{VRES,total}} + 100\%\right) \cdot P_{export,max} \quad \forall t \tag{2.11j}$$

$$P_{export}(t), P_{import}(t) \leq P_{export,max} \quad \forall t \tag{2.11k}$$

$$P_{export}(t) \cdot P_{import}(t) = 0 \quad \forall t \tag{2.11l}$$

Although the the problem statement above might seem like classical optimisation problem, another approach is taken in this thesis.

First, Equations (2.11b), (2.11c), (2.11f), (2.11k) and (2.11l) are handled by the internal model logic. Equations (2.11h) and (2.11j) are used together after a simulation has ended, in order to determine what portion of the exported energy has been sold to neighbouring countries, generation annual revenue. Since energy that could not be sold can always be curtailed, these constraints can always be met. Using them as constraints in the optimiser would mean that for simulations with high overproduction factors, the amount of storage would have to increase in order to be able to store all the enrgy

Equations (2.11g), (2.11i) and (2.11k) are used as constraints for the storage optimiser. The optimal amount of storage for each simulation is determined by using the same root-finding algorithm as is used for finding the total solar surface area. Specifically, the root-finding algorithm called ”Brent’s method”. However, since this algorithm’s goal is to find the roots of a given function, we can not use it to determine the amount of storage directly. To overcome this problem, the remaining constraint are restated, such that when they are satisfied they will have a root at the respective storage capacity. This behaviour of the constraints is achieved by dividing the desired value of each constraint by the value found during a simulation and subtracting 1. In essence, this normalises the constraints, and it will result in a negative value when the constraint is satisfied. for Equation (2.11e) the difference between the SOC at the start and end is calculated, and logic is implemented that outputs 1 when the SOC is lower at the end, and -1 if the SOC is equal or higher, signalling the constraint has been met. The object function has been formulated in such a way that it will return the highest value of the normalised constraints. The root finding algorithm then finds the minimal amount of storage needed for all constraints to be at or below

zero. The taken approach however only works when all constraints are monotonically decreasing for increased storage capacities, which is proven in Section 2.9.2.

2.8. System Cost and Revenue

This section describes the calculation of the yearly total system cost for the different simulations. The goal of calculating the system cost is to asses whether the Low-Wind turbine could be a cost-effective solution for the different scenarios. The system cost does not contain the cost of all components in the system, as this is not deemed either necessary or feasible. Components in the system that are constant for each simulation are omitted, since the cost of these components do not affect the which combination of offshore conventional turbines, Low-Wind turbines and storage capacity results in minimum costs. Since the size of the onshore wind turbines and PV generation remains unchanged between the different scenarios, their costs will be the same as well, and are therefore not of interest. The price for both the imported and exported energy is set at 0.72 €/MWh (CBS, 2021). For this study it is assumed that the transmission and distribution grid within the Netherlands is able to handle a high VRES penetration and that it will remain constant between the simulations.

The power system also generates revenue by exporting energy to neighbouring countries, while the import of energy incurs extra costs. Cost figures for the components used in this model have been described in the sections above. However, these costs have been divided in capital expenditures (CAPEX) and operational expenditures (OPEX). For simplicity all costs are calculated on a per-year basis, so that they can be added together into a single parameter for each simulation. The yearly cost of an individual component is calculated using Equation (2.12):

$$c_{component,y} = \frac{c_{component,CAPEX}}{a} + c_{component,O\&M} \tag{2.12}$$

Where $c_{component,CAPEX}$ is the CAPEX of the component, a the annuity factor and $c_{component,O\&M}$ the component OPEX. The annuity factor can be calculated using Equation (2.13) (M. B. Zaayer, 2000):

$$a = \sum_{n=1}^{N} (1+r)^{-t} = \frac{1 - \left(\frac{1}{1+r}\right)^{T'}}{r} \tag{2.13}$$

where N is the number of components, r is the real interest rate and T' is the economic lifetime of the component after construction. In this study the real interest rate r is set at 10 % (Renewable Energy World, 2021). The cost of the different scenarios composes of the sum of the cost of all components, costs incurred from the needed import of energy minus the revenue generated from export of energy, as shown in Equation (2.14):

$$c_{total} = \sum_{1}^{n=N} \left(c_{component,n}\right) + c_{O\&M,system} + c_{import} \cdot E_{import} - c_{export} \cdot E_{export} \tag{2.14}$$

where N is the number of components, $c_{component,n}$ is the cost of component n,$c_{O\&M,system}$ are the O&M costs of the energy system, c_{import} is the cost of a unit of imported energy, E_{import} is the annual imported energy, c_{export} is the price received for exported energy and E_{export} is the annual exported energy.

2.9. Model Verification

This section describes the verification of the model that is created during and for this thesis, and shows that the implemented optimisation approach has the desired behaviour. Only the system behaviour and optimisation are verified. The cost modelling is not verified here, but is a subject of the sensitivity study. The goal of this section is to show that the power model and optimisation work as intended, and can be used for the generation of the results. Section 2.9.1 demonstrates the behaviour of the model, by showing data from a single, arbitrary run. Section 2.9.2 shows the behaviour of the constraints that have been implemented in the optimisation, in order to validate that an optimum storage capacity can be found using the chosen approach.

2.9.1. Power model behaviour

This section shows that the power model designed for this thesis works as intended. The settings for the simulation are 1500 conventional offshore turbines and a storage capacity of 1×10^5 MW h. This is not considered optimal, but these settings are chosen for demonstration purposes. The chosen amount of turbines results in a slight annual overproduction, while the storage capacity is smaller than actually needed. The storage has a minimum and maximum SOC of 0.2 and 0.8, respectively. The chosen combination of storage capacity for the amount of turbines ensures that import and export will occur more frequently, while the battery also reaches its set minimum and maximum SOC often, in order to show that the model-logic is correct. Figure 2.7 shows the time series for the first week of a single simulation.

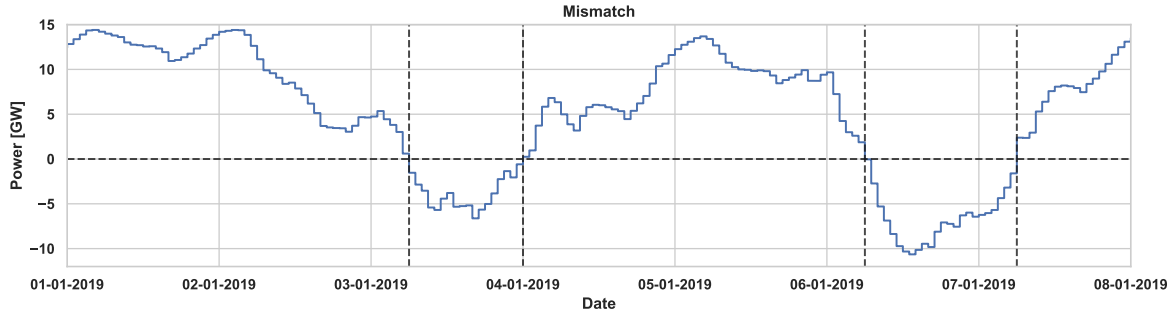

(a) Mismatch during the first week

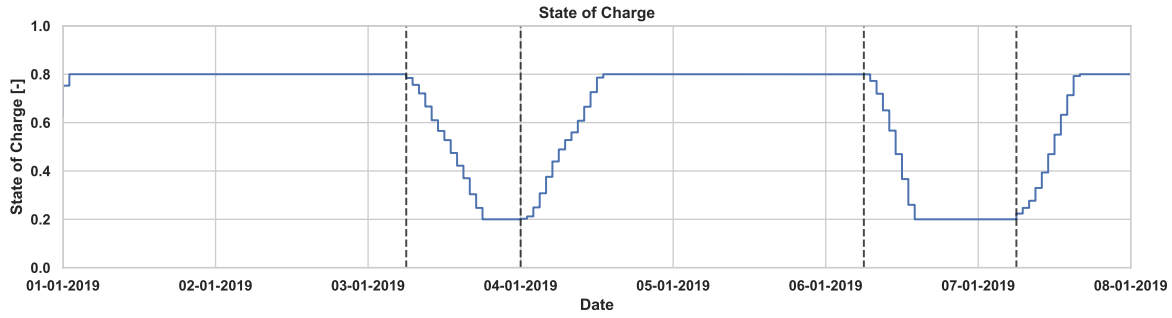

(b) Battery SOC during the first week

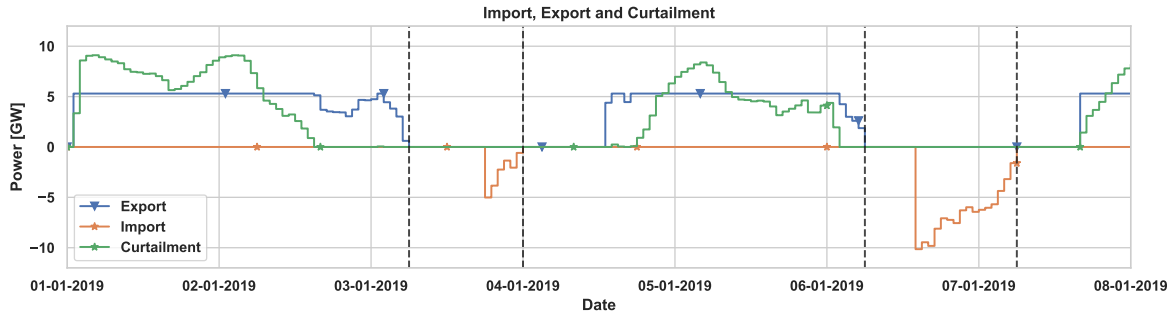

(c) Import and export during the first week

Figure 2.7: Graphs showing power model behaviour during the first week of a simulation

Figures 2.7a to 2.7c show the mismatch between supply and demand, SOC of the storage and export and import data for the first week of the simulation, respectively. The vertical dashed lines indicate moments in the time series where the mismatch switches from positive to negative. Looking at Figure 2.7a, it can be seen that for moments where the mismatch is negative, the SOC starts dropping, which means the storage is supplying energy to the system in order to meet demand. Then, when the storage reaches it minimum SOC and can not be used anymore, energy needs to be imported into the system, which can clearly be seen happening in Figure 2.7c. During moments of positive mismatch,

meaning a surplus of energy, the opposite behaviour can be seen. First, the storage charges up to its maximum SOC, after which the rest of the energy is either exported to neighbouring countries or curtailed. From Figure 2.7c we can also deduce that import and export or curtailment never happen at the same moment.

2.9.2. Optimisation Constraint Behaviour

Figures 2.8a, 2.8b and 2.8c show plots of the constraints used to optimize storage capacity.

Figure 2.8a shows the behaviour of the constraint on the annual import, stated in Equation (2.11g). The curves show that, for increasing storage capacity, the amount of annual import decreases, which is as expected. Increasing the storage capacity ensures more of the generated energy can be stored, reducing the need for import. Also, for increased generation capacity the lines shift to the left, which is also expected behaviour. Having more energy available in the system means there are fewer moments of mismatch and the system has enough energy in storage more often, so it becomes less reliant on import of energy.

Figure 2.8b shows the behaviour of the constraint on the maximum instantaneous import, stated in Equation (2.11i). In this graph it can be seen that the individual lines switch from positive to negative quite abruptly. The abrupt change can be caused by the fact that a certain point in the time series is normative, and once a large enough storage capacity solves this point the constraint is satisfied. This indicates that the model might be very sensitive to this constraint. Again we see than for increasing installed generation the curve shift to the left, reducing the storage capacity needed to satisfy the constraint. However, this effect becomes marginal for further overproduction, since all curves are very close together.

Figure 2.8c shows the behaviour of the constraint on the physically allowable import constraint, stated in Equation (2.11k). The shapes of the curves are similar to the previous graph, which is to be expected since the constraints are also quite similar. This constraint also demonstrated the same abrupt characteristics as the previous constraint.

From the graphs we can conclude that all constraints are monotonically decreasing, making them suitable to use in the root-finding algorithm. The abrupt nature of the constraints was not expected, but the exact cause of this is not investigated in this study.

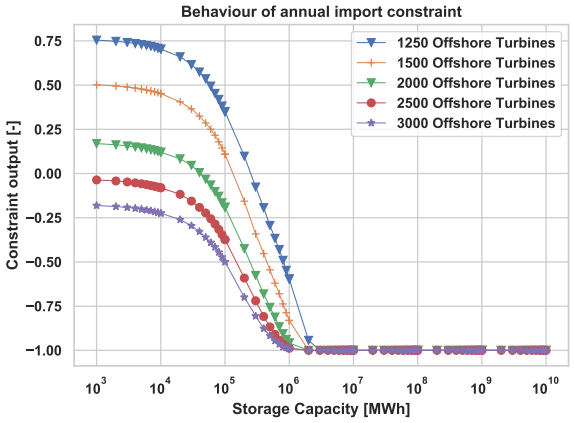

(a) Behaviour of annual import constraint,Equation (2.11g), for different storage capacities and installed offshore capacity

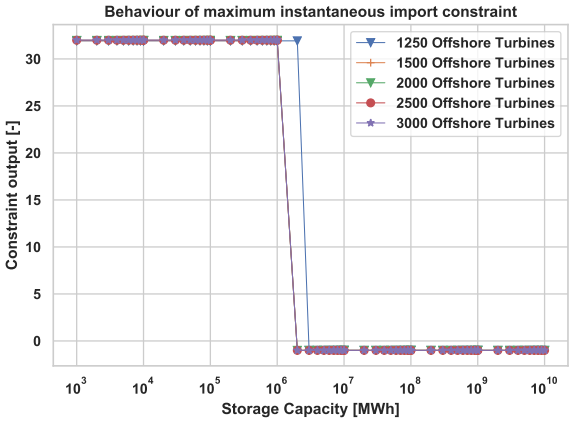

(b) Behaviour of instantaneous import constraint, Equation (2.11i)„ for different storage capacities and installed offshore capacity

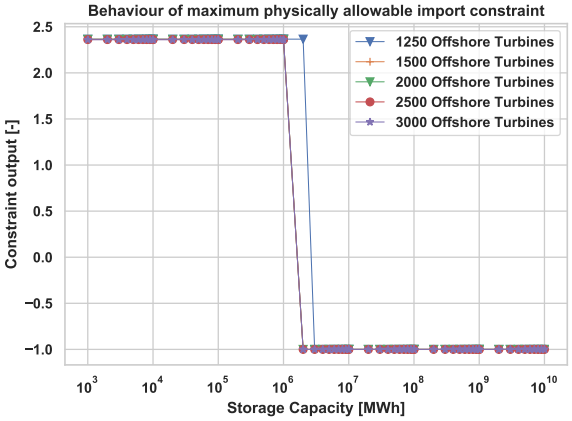

(c) Behaviour of physically allowable import constraint, Equation (2.11k), behaviour for different storage capacities and installed offshore capacity

Figure 2.8: Graphs showing the constraint behaviour for different storage capacities and different amount of installed offshore turbines

3

Low-Wind Turbine: Cost and Scaling Model Description

This chapter describes the model that was used in order to design the Low-Wind Turbine. The goal behind the model is to calculate the cost of the scaled components and determine the cost of the Low-Wind Turbine. Section 3.1 shows a flowchart of the Low-Wind Turbine model, to visualize the different parts of the model. Section 3.2 describes the rationale behind the modelling choices. Section 3.3 describes how the data of the reference turbine is acquired and used. Section 3.4 describes the scaling rules applied to the blades. Section 3.5 describes the determination of the mass and cost of the direct drive generator Section 3.6 describes the redesign of the wind turbine tower.

The blades have to be adjusted, so they still operate at optimum performance at the new rated wind speed and TSR, explained in Section 3.4. The new chord lengths result in a different blade mass. The direct drive generator mass and cost are scaled, based on the new torque in the low speed shaft (LSS), explained in Section 3.5. The tower dimensions are scaled under the assumption that the compression stress at the top of the tower and the bending stress at the bottom of the tower have to be kept constant, explained in Section 3.6.

3.1. Model Flowchart

Figure 3.1 shows a flowchart of the Low-Wind Turbine scaling model. The Flowchart is read from left to right and top to bottom.

The Low-Wind Turbine Scaling model is separated into four different components, indicated by the square blue blocks in the flowchart. The major components of the model are the scaling models for the blades, generator and tower and the calculation of the total Low-Wind turbine Cost. The slanted orange blocks on the left-hand side of the flowchart indicate the data of the reference turbine that is imported into the model, while the slanted green block indicate output data of the different modelling components.

3.2. Rationale

The goal of the scaling rules in the following sections is to determine the cost of the Low-Wind Turbine, while also having a feasible preliminary turbine design. The Low-Wind Turbine is designed by taking a reference turbine and applying scaling rules to several wind turbine components. Reference wind turbines are theoretical wind turbines with publicly available designs, specifically developed for research purposes.

The rated power of the wind turbine is reduced by reducing the rated wind speed, in order to make it a Low-wind Turbine. According to Blade Element Momentum theory (BEM) the rated power P_{rated} of a turbine can be calculated using Equation (3.1):

$$P_{rated} = \frac{1}{2}\eta_{turbine} \cdot c_p \cdot \rho_{air} \cdot \frac{1}{4}\pi \cdot D_{rotor}^2 \cdot U_{rated}^3 \tag{3.1}$$

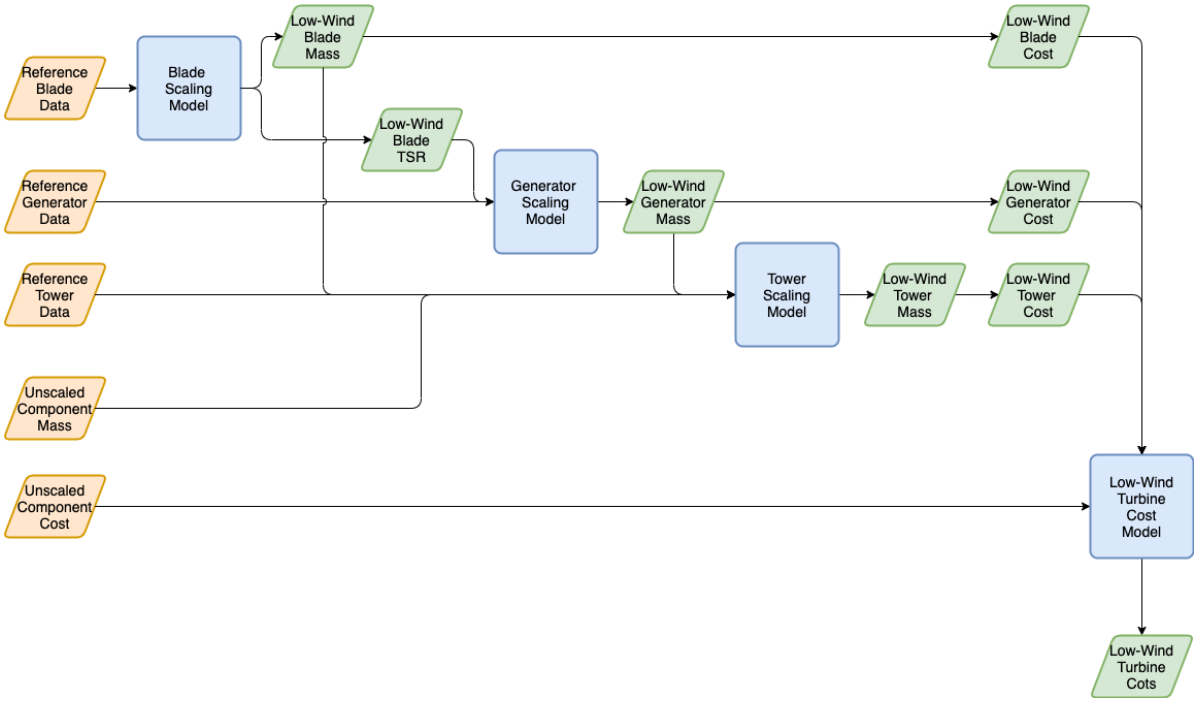

Figure 3.1: Flowchart showing Low-Wind Turbine Modelling Components

where $\eta_{turbine}$ the total turbine efficiency, c_p the turbine power coefficient, ρ_{air} the air density, D_{rotor} the turbine rotor diameter and U_{rated} the turbine rated wind speed. Using this equation, a rated power P_{rated} can be determined for a given rotor diameter and rated wind speed. During scaling the rotor diameter is kept constant as to not stray from the original design length. The turbine power coefficient c_p is kept constant at the same value as the reference turbine, since the scaling of cord and twist ensures unchanged aerodynamic performance. The reduced rated wind speed results in lower loads on the wind turbine. In turn, the reduction of the loads on the turbine create room in the design to reduce the amount of material needed, which in turn reduces the cost of the scaled components.

The redesign of the components changes their mass, and the mass of the components is used to determine the cost. In the case of the tower top, the mass of all the components supported by it is needed to calculate the compression stress. The components which mass and cost are scaled in this thesis are the blades, direct drive generator and the tower. An overview of the main components of the Low-Wind Turbine, their respective design drivers and design variables are shown in Table 3.1.

Table 3.1: Overview of main Wind turbine Components, their respective design driver and design variables

Component	**Design drivers**	**Design Variables**
Blades	Aerodynamic performance, Stress, Tip deflection	U_{rated}, λ_{rated}
Generator	Torque	U_{rated}, λ_{rated}
Tower	Thrust, RNA-weight	U_{rated}
Gearbox	Not Applicable	
Controller	None	
Rotor Hub	None	
Transformer	None	
Nacelle	None	
Other	None	

At the time of writing this thesis, the IEA 15 MW reference wind turbine (Gaertner et al., 2020a) is the reference wind turbine with the largest rotor diameter of which sufficient information is publicly available, making it a viable starting point for the design of the Low-Wind Turbine concept. During this thesis the

IEA 15 MW reference wind turbine serves two roles. The first role is providing a design that is adjusted by applying scaling rules, in order to design the Low-Wind Turbine. The second role is providing cost- and mass-figures, which are used to determine the cost of the Low-Wind Turbine, either by applying scaling relations to the cost- and mass-figures or using them unchanged for the components that are not scaled.

Due to the limited time and scope of this thesis it is not deemed either feasible or necessary to calculate the mass and cost of every Low-Wind Turbine component. The exact cost of each individual component is not of extreme importance as this thesis focuses on the big picture of the entire Dutch energy grid. Furthermore, not all component mass and/or cost scale with thrust, power, rotational speed or other parameters. The exact mass and cost of the unscaled components are considered to be of less importance to the overall cost of the turbine.

3.3. Acquisition and Use of Reference Turbine Data

The IEA 15 MW reference turbine data used in this model come from three different sources in order to provide sufficient data. The report (Gaertner et al., 2020a) explains the turbine design and gives information about the performance. The IEA Wind Task 37 online Github repository (Gaertner et al., 2020b) provides datasheets with designs of the turbine components, as well as some component masses. However, these two sources do not provide information about the cost of the turbine or any of its components. For the cost figures of the IEA 15 MW RWT, WISDEM is used (NREL, 2020). The input data that was used to generate the data can be found on the IEA Wind task 37 Github repository (Gaertner et al., 2021). When this thesis states data that was generated using WISDEM and the input data, it will be stated as such and referenced using: (NREL, 2020; Gaertner et al., 2021).

3.4. Blades

This section describes the modelling steps for the turbine blades. The goal behind the blade scaling is to minimise the blade cost by reducing its material use, while adjusting the chord and twist to ensure the blade still operates at its original design point. Section 3.4.1 explains the scaling laws for the different blade parameters, properties and loads on the blade. Section 3.4.2 describes a self-derived blade cost equation. Section 3.4.3 gives an overview of the blade optimisation philosophy.

3.4.1. Blade Scaling

The Low-Wind Turbine is based off of a reference turbine, by applying the scaling rules mentioned in the following sections. The scaling rules can be used to scale the blade properties for a change in rated wind speed U_{rated}, design Tip Speed Ratio (TSR) λ_{design} and thickness factor f_t. These parameters, and their effect on blade properties are explained in the sections below. A lower rated wind speed results in a reduction of loads on the blades, which in turn results in a reduction of stress in the material. This stress reduction enables a re-design of the blades to decrease the amount of material used, and therefore reduce the cost of the blade.

3.4.1.1. Tip Speed Ratio

The design TSR is constrained by the maximum tip speed of the reference turbine at rated wind speed, due to noise regulations and blade erosion. Blade erosion occurs because the blade leading edge is impacted with various projectiles, such as rain and hail droplets(Keegan et al., 2013). Higher tip speeds lead to higher impact velocities and thus increased leading edge damage over time. In turn, erosion of the leading edge leads to decreased aerodynamic performance over time. The scaled blade uses the same materials as the reference turbine, so its is assumed that it is able to withstand the same impact velocities. The TSR is calculated using Equation (3.2):

$$\lambda_{design} = \frac{(\Omega_{rated} R)}{U_{rated}} \propto U_{rated}^{-1} \tag{3.2}$$

Where λ_{design} is the design TSR, Ω_{rated} is the rotational speed at rated wind speed, R is the rotor diameter and U_{rated} is the turbine rated wind speed. As will be explained later in Section 3.4.1.4, increasing the TSR is beneficial to reduction of blade mass, which decreases its capital costs. Another benefit of increasing the TSR is that it reduces the torque in the LSS, and thereby the cost of the generator, which is made clear in Section 3.5.2.

3.4.1.2. Chord and Twist

Changing the TSR of the blade changes the velocity triangles of the airfoils. To ensure that the blade operates at optimal performance for the new TSR, the chord and twist of the blade are adjusted. Equation (3.3) is used to adjust the chord of the turbine blade (Canet et al., 2020):

$$c = \frac{16}{9}\frac{\pi}{Bc_l\lambda^2}\left(\frac{r}{R}\right)^{-1} \cdot R \propto \lambda^{-2} \tag{3.3}$$

where c is the chord length, R is the blade length, B the number of blades, c_l the lift coefficient, λ the TSR and $\left(\frac{r}{R}\right)$ the airfoil radial position along the blade. Equation (3.4) is used to adjust the twist of the blade, where α_{design} is the airfoil design optimum angle of attack.

$$\theta + \alpha_{design} = \frac{2/3}{\lambda\,(r/R)} \propto \lambda^{-1} \tag{3.4}$$

3.4.1.3. Blade Stiffness

Changing the chord and twist also has an effect on the structural properties of the blade. The strength and stiffness of a component is determined by its used materials and geometric shape. The stiffness of is defined as $E \cdot I$, where E is Young's modulus, and I the area moment of inertia. E is a material property, while I is a geometrical property. Since the blade will use the same materials as the reference, the change in its strength and stiffness will result from changes in geometry, which changes its area moment of inertia I. The structural components of the blade are the spar caps and shear webs, as shown in Figure 3.2.

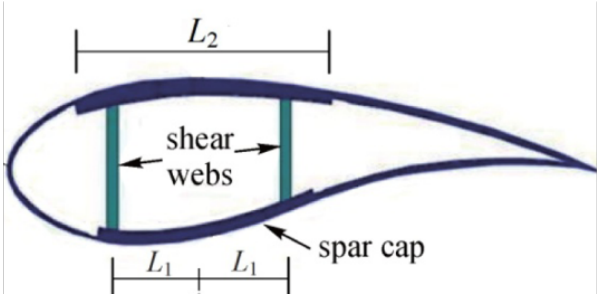

Figure 3.2: Schematic Representation of a Turbine Blade Cross-Section

The area moment of inertia of the blades can not easily be determined exactly. For the derivation of this blade property we look at the changes that occur to the blade cross-section, and use a thin shell approximation. From Equation (3.3) we know that $c \propto \lambda^{-2}$. Since all dimensions of an airfoil are a function of its chord length, we can use this property to scale its area moment of inertia. the area moment of inertia is calculated using Equation (3.5):

$$I = \iint y^2 dA \propto c^4 \propto \lambda^{-8} \tag{3.5}$$

Where y is the perpendicular distance of element dA to the neutral axis. Using thin shell approximation, the blade element dA is modelled as a line element with length dl and thickness t, and it calculated using Equation (3.6). When a thickness factor f_t is introduced, this can be rewritten as Equation (3.7). The thickness factor f_t is defined as a factor that scales the thickness of the laminates equally. with the thickness factor the strength of the blade can be adjusted up and down easily, without changing its aerodynamic shape and therefore its performance. This thickness factor can be used in the optimisation of the blade.

$$dA = t \cdot dl \propto c^2 \tag{3.6}$$

$$dA_{f_t} = f_t \cdot t \cdot dl \tag{3.7}$$

Since a thin shell approximation is used, the thickness t will be small. Therefore, Applying a thickness factor will not have an effect on the position of the line element and does not affect distance y either. summarising the information above, Equation (3.5) can be rewritten as Equation (3.8).

$$I_{f_t} = \iint y^2 dA_{f_t} = \iint y^2 \cdot f_t \cdot dA = f_t \cdot I \tag{3.8}$$

$$I_{f_t} \propto \lambda^{-8}, f_t \tag{3.9}$$

3.4.1.4. Blade mass

Scaling of blade mass is also based on the scaling of the blade cross-section. Since the blade length is kept constant during this study, the proportionality $A_{cross-section} \propto c^2$ is used. From Equation (3.3) we know $c \propto \lambda^{-2}$. This results in a proportionality for the cross-sectional area: $A_{cross-section} \propto \lambda^{-4}$. Using this information and the definition for the thickness factor f_t, described in Section 3.4.1.3, the mass of a blade can be calculated using Equations (3.10) and (3.11):

$$m_{blade} = \sum_{1}^{i} dr_i \cdot \mu_{blade,i} \propto f_t, \lambda^{-4} \tag{3.10}$$

$$\mu_{blade,i} = \rho_i \cdot f_t \cdot A_{cross-section,i} \propto f_t, \lambda^{-4} \tag{3.11}$$

where m_{blade} is the total blade mass, i is the number of blade sections, dr_i is the section length, $\mu_{blade,i}$ is the mass per unit length, ρ_i is the blade section mass density,f_t is a thickness factor, and $A_{section,i}$ is the cross-sectional area for each blade section i.

3.4.1.5. Thrust force

Using BEM, the thrust the rotor exerts on the flow is determined using Equation (3.12). A wind turbine rotor exerts the highest thrust on the airflow at rated wind speed, and therefore the blades experiences the highest loads at these conditions. The trust force is determined as follows:

$$T_{rated} = \frac{1}{2}\rho c_t \pi R^2 U_{rated}^2 \propto U_{rated}^2 \tag{3.12}$$

where ρ is the density of air, c_t is the thrust coefficient, R is the rotor diameter and U_{rated} is the rated wind speed.

3.4.1.6. Moments and Stresses

The blade experiences two main forces which cause moments in the blades. The first one is caused by aerodynamic loading of the blade, while the second is caused by the self-weight of the blade. The moments on the blade are determined by:

$$M_{aero} = \int_0^R F_{aero}(r) \cdot r dr \propto U_{rated}^2 \tag{3.13}$$

$$M_{gravity} = \int_0^R F_{gravity}(r) \cdot r dr \propto f_t, \lambda^{-4} \tag{3.14}$$

where M_{aero} is the moment caused by aerodynamic loading and $M_{gravity}$ is the moment caused by gravitational loading on the blades. Again the blade length is unchanged during this thesis, so the moment-arm is not affected. However, the forces acting on the blade are changed, because the rated wind speed is decreased and the blade mass is changed as a result of a change in chord length. The aerodynamic moment M_{aero} is related to the trust force $T_{rated} \propto U_{rated}^2$ and is in the out-of-plane direction, while the gravitational moment $M_{gravity}$ is related to the blade mass $m_{blade} \propto f_t, \lambda^{-4}$ and is in the in-plane direction of the rotor. The moments in the blade cause stresses in the blade material, which are expressed in Equations (3.15) and (3.16).

$$\sigma_{aero} = \frac{M_{aero} \cdot y}{I} \propto U^2, \lambda^6, f_t^{-1} \tag{3.15}$$

$$\sigma_{gravity} = \frac{M_{gravity} \cdot y}{I} \propto U_{rated}^2, \lambda^2, f_t^0 \tag{3.16}$$

3.4.1.7. Tip Deflection

The out-of-plane tip deflection of the wind turbine blade is the main design driver for large wind turbine blades. the deflection of the blade as a function of radial position r can be determined with Equation (3.17):

$$y_{tip}(r) = \int_0^r \int_0^x \frac{M_{aero}(x')}{EI(x')} dx' dx \propto \lambda^8, U^2, {f_t}^{-1} \tag{3.17}$$

3.4.2. Blade Cost

The cost of the scaled blade is determined by its change in mass, which translates to a reduction in material costs. All other costs will remain constant. Using the outcome of the blade cost model integrated in NREL Wind-Plant Integrated System Design and Engineering Model (WISDEM) (P. Bortolotti et al., 2019), a cost breakdown can be found for three different blade types and lengths. This Thesis focuses on turbines with large rotor diameters, so the cost breakdown of the SNL-100-03 blade, which has been developed by Sandia National Laboratories (SNL), is taken as a reference point. The SNL-100-03 is 100 m long, made with carbon fibre spar cap, has a mass of around 50×10^3 kg, costs around 548×10^3 \$, 624×10^3 €, of which the material cost comprise around 323×10^3 \$, 368×10^3 €. Dividing the material cost by the total cost shows that 59 % of the blade cost are material costs. Figure 3.3 shows a pie-chart of the cost breakdown of the SNL-100-03, which confirms the result for the material cost share.

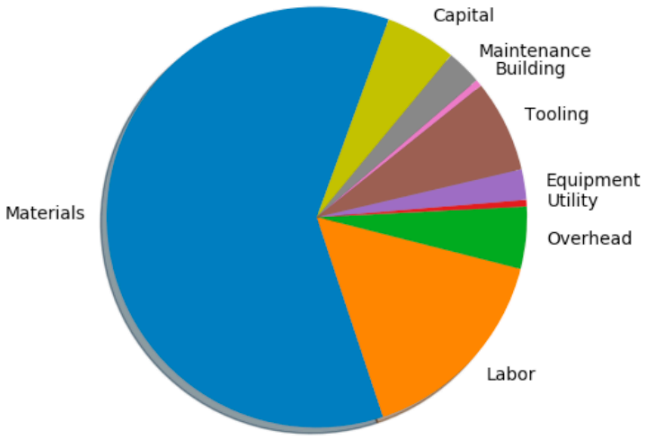

Figure 3.3: Pie Chart Showing Cost Breakdown of SNL-100-03 (P. Bortolotti et al., 2019)

Using the information above, a cost formula for the scaled blade is derived. It is assumed that the cost of the used reference turbine follows the same breakdown as the SNL-100-03 blade and that the only change in blade cost is a result of change in amount of material used. As mentioned earlier, the other costs for the blade are assumed to be constant. The blade cost is determined by Equation (3.18):

$$c_{blade,new} = \left(\frac{m_{blade,new}}{m_{ref.blade}} \cdot 0.59 + 0.41 \right) \cdot 625 \times 10^3 \tag{3.18}$$

where $c_{blade,new}$ is the cost of the new blade, m_{blade} is the mass of the new blade, $c_{ref.blade}$ is the reference blade cost and $m_{ref.blade}$ is the reference blade mass.

3.4.3. Blade Optimisation

The equations and scaling rules mentioned above are used to design a new blade for the Low-Wind turbine. As mentioned, the goal of the new design is to minimise material use by designing a lightweight blade. However, the blade still has to be strong enough to withstand the stresses. The aim of the re-design is to keep the stresses and tip deflection of the blade equal to the reference turbine. Summarising the equations described above we have Equations (3.19) to (3.21).

$$\sigma_{aero,new} = \left(\frac{U_{new}}{U_{old}}\right)^2 \left(\frac{\lambda_{new}}{\lambda_{old}}\right)^6 \cdot f_{t,new}^{-1} \cdot \sigma_{aero,old} \tag{3.19}$$

$$\sigma_{gravity,new} = \left(\frac{U_{new}}{U_{old}}\right)^2 \left(\frac{\lambda_{new}}{\lambda_{old}}\right)^2 \cdot \sigma_{gravity,old} \tag{3.20}$$

$$y_{tip,new} = \left(\frac{U_{new}}{U_{old}}\right)^2 \left(\frac{\lambda_{new}}{\lambda_{old}}\right)^8 f_{t,new}^{-1} \cdot y_{tip,old} \tag{3.21}$$

The equations in this section are used to design the blade for the Low-Wind Turbine. The blade is scaled from a reference turbine and the TSR and thickness factor are adjusted to keep the stresses in the blade lower then, or equal to the reference design, optimising for lowest blade mass. the conditions that must be met are stated in Equations (3.22) to (3.24).

$$\sigma_{aero,new} \leq \sigma_{aero,old} \tag{3.22}$$

$$\sigma_{gravity,new} \leq \sigma_{gravity,old} \tag{3.23}$$

$$y_{tip,new} \leq y_{tip,old} \tag{3.24}$$

from the Equations (3.19) to (3.21) it can be concluded that the stresses in the material and tip deflection are strongly proportional to TSR. Especially y_{tip}, which is proportional to λ^8, will be the dominant design driver. Although the stress and deflection can be counterbalanced by applying very high thickness factors, this is not considered a feasible design approach, as this will increase the blade mass and therefore its cost. For this reason, the thickness factor is kept at unity when optimising the blade TSR.

3.5. Generator

For the generator of the low-wind turbine a direct drive is chosen, based on the IEA 15 MW reference turbine. As already mentioned, this currently is the reference wind turbine with the largest rotor diameter. The IEA 15 MW reference wind turbine has a direct drive generator. The Low-Wind Turbine will also be designed with a direct drive generator, in order to stay as close to the reference turbine as possible.

3.5.1. Generator Torque

The torque in a direct drive generator is equal to the aerodynamic torque in the rotor. The rotor torque is defined as:

$$Q_{rotor,max} = \frac{1}{2} c_Q \rho_{air} \pi R^3 U_{rated}^2 \tag{3.25a}$$

$$c_Q = \frac{c_p}{\lambda} \tag{3.25b}$$

$$Q_{rotor,max} \propto U_{rated}^2, \lambda^{-1} \tag{3.25c}$$

where c_Q is the torque coefficient, ρ_{air} is the density of air, R is the rotor radius and U_{rated} is the rated wind speed of the turbine. The same c_p as the reference turbine is used in Equation (3.25b), since the blade chord and pitch are adjusted in order to keep operating at the optimal conditions.

3.5.2. Generator Mass

The turbine generator mass scales linearly with the rotor torque, according to ”DrivetrainSE” documentation of WISDEM (NREL, 2019a). Using this assumption, a new function is created with the available data

from the IEA 15 MW reference turbine. This reference direct-drive generator has a rated torque of 18.97 MN m, and a mass of 372 kt (Gaertner et al., 2020b), resulting in a specific mass of 19.61 kg/(Nm)

$$m_{generator,DD} = 19.61 \cdot Q_{rotor,max} \propto U_{rated}^2, \lambda^{-1} \tag{3.26}$$

Where $m_{generator,DD}$ is the direct-drive generator mass in kg and Q_{rotor} is the rotor torque in N m. with this equation the new generator mass is can be determined by scaling from the reference turbine generator mass.

3.5.3. Generator Cost

According to the NREL Cost and Scaling model , the cost of the generator is directly related to its power rating (Fingersh et al., 2006). The 2006 report states a price of 219.33 $/kW, which equates to 288.94 $/kW in 2020 USD, or 329.39 €/kW. WISDEM determines a price for IEA 15 MW reference turbine generator of around 160 $/kW (NREL, 2020; Gaertner et al., 2021), or 182 €/kW. A BVG associates report states a price of 2×10^6 £ for a 10 MW direct drive generator (BVG Associates, 2019), resulting in a cost of 200 £/kW, or 224 €/kW. The three prices give an indication of the general cost of a direct drive turbine, however we can not assume one of them to be accurate, due to advancements in technologies and economy of scale. Because of this, the average of the three prices is taken as the direct drive cost figure in this study, resulting in a price of roughly 245 €/kW. The cost of the wind turbine can now be calculated using Equation (3.27):

$$c_{generator,DD} = 245 \cdot P_{generator,DD} \tag{3.27}$$

3.6. Tower and Monopile

The sections below describe the modelling steps taken for the redesign of the tower. Section 3.6.1 describes the rationale behind the modelling steps. In Section 3.6.2 the scaling rules applied to the tower top and bottom are explained, as well as how those outcomes result in the tower design. Section 3.6.5 describes the calculation of the natural frequency of the tower. Section 3.6.3 describe how the mass and cost of the new tower is calculated.

3.6.1. Rationale

The tower of the reference turbine is scaled while accounting for the change in static loading on the structure. The aim of the redesign is to keep the stress in the material of the tower base and top constant to the reference tower, while avoiding buckling. Figure 3.4 gives an overview of the different loads that act on the tower and the foundation. The wind turbine tower starts at platform height and goes up to the base of the nacelle. The foundation is considered to be everything below the platform. In this study the foundation consists of a monopile. Between the monopile and the wind turbine tower is a transition piece, which connects the two together. The monopile is considered to remain unchanged to the original design.

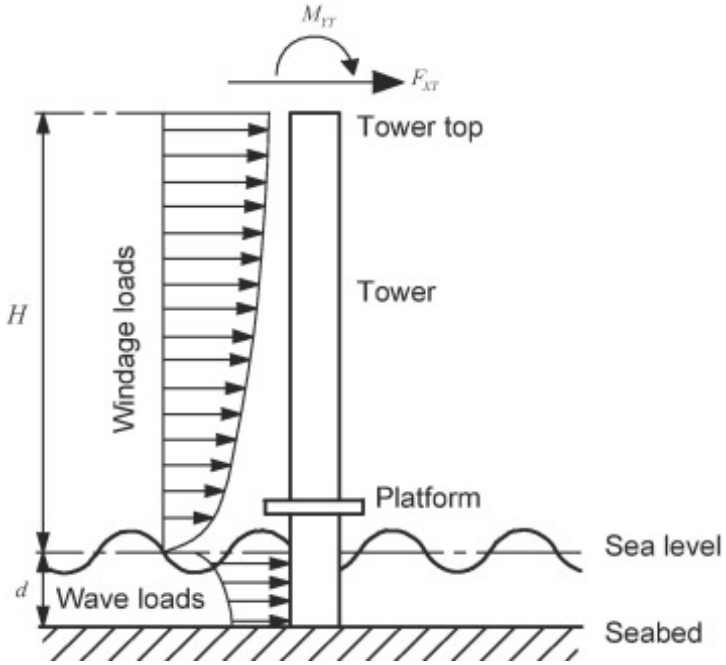

Figure 3.4: Schematic Overview of Loads on Wind Turbine Tower (Harlan et al., 1996)

Two load-cases are considered for the redesign, namely the load-case at the top of the tower and the load-case at the bottom of the tower. Buckling is avoided by keeping the ratio of the wall thickness to outer diameter constant. At the tower base, loading is considered to be dominated by the moment caused by the rated thrust force T_{rated}. At the tower top, loading is considered to be dominated by the compressive force, caused by the mass of the rotor nacelle assembly (RNA). The change in dynamic loading of the tower is beyond the scope of this research. Since only the change in static loading is considered, the tower is considered an imperfect design. The natural frequency of the redesigned tower is calculated and checked for coincidence with the 1P and 3P harmonics. If the scaled tower natural frequency coincides with the 1P and 3P harmonics, this is noted, but the tower design will not be adjusted. However, for a first-order approximation of tower cost this approach is considered sufficient.

3.6.2. Tower scaling

This section describes the scaling rules applied to the tower. First, the rules for the tower base are explained. Then, the rules for the tower top are explained. Lastly it is explained how the outcomes for the tower base and top result in a new tower design.

3.6.2.1. Tower Base

At the tower base, the loading is considered to be dominated by the thrust force T, which is determined using Equation (3.12). Equation (3.28) is used to calculate the bending stress $\sigma_{tower,base}$ in the tower base,

$$\sigma_{tower,base} = \frac{M_{tower,base} \cdot y}{I_{tower,base}} \tag{3.28}$$

where $M_{tower,base}$ is the moment acting on the tower base, y is the perpendicular distance from the neutral axis and $I_{tower,base}$ is the area moment of inertia of the tower base. The moment in the tower base is a function of the thrust force T and tower length L_{tower}. From Equation (3.12) we know that $T_{rated} \propto U_{rated}^2$. As the rotor Diameter is not changed in this thesis, the tower length L_{tower} is also kept constant.

$$M_{tower,base} = T \cdot L_{tower} \propto U_{rated}^2 \tag{3.29}$$

The perpendicular distance from the neutral axis y is equal to the tower radius or half the tower diameter and we can state its proportionality as follows:

$$y = 0.5D_{outer} \propto D_{outer} \tag{3.30}$$

The individual tower segments are designed as thin walled hollow cylinders. The area moment of inertia is calculated with Equation (3.31):

$$I_{cyl} = \frac{\pi}{64}\left(D_{outer}^4 - D_{inner}^4\right) \tag{3.31}$$

where D_{outer} and D_{inner} are the tower outer and inner diameter, respectively. The inner diameter can also be expresses as a function of the outer diameter and wall thickness t_w, stated in Equation (3.32).

$$D_{inner} = D_{outer} - 2 \cdot t_w \tag{3.32}$$

As stated, the ratio of the tower outer diameter and wall thickness is kept constant to avoid buckling. The wall thickness can be described using Equation (3.33),

$$t_w = D_{outer} \cdot \frac{t_w}{D_{outer}} = D_{outer} \cdot \Theta \tag{3.33}$$

where Θ is defined as the ratio between wall thickness and outer diameter. The inner diameter can be rewritten as a function of the outer diameter and Θ.

$$D_{inner} = D_{outer}\,(1 - 2 \cdot \Theta) \tag{3.34}$$

Equation (3.31) can be rewritten as Equation (3.35). Ultimately, rearranging the equation results in Equation (3.36), from which the proportionality $I_{cyl} \propto D_{outer}^4$ is derived.

$$I_{cyl} = \frac{\pi}{64}\left(D_{outer}^4 - \left(D_{outer}\,(1 - 2 \cdot \Theta)\right)^4\right) \tag{3.35}$$

$$I_{cyl} = \frac{\pi \cdot D_{outer}^4}{64}\left(1 - (1 - 2 \cdot \Theta)^4\right) \propto D_{outer}^4 \tag{3.36}$$

summarising all the information stated above, the scaling law for the tower base bending stress is stated in Equation (3.37)

$$\sigma_{tower,base} \propto U_{rated}^2, D_{outer}^{-3} \tag{3.37}$$

3.6.2.2. Tower Top

The tower top scaling is based on compression stress $\sigma_{tower,top}$. This compression stress is a result of the mass of all the components that are supported by the tower. These components consist of the following components: blades, hub, generator, bed-plate and miscellaneous components. As with the the tower base, the goal of the scaling relations is to keep the bending stress constant. the stress in the tower top is determined by:

$$\sigma_{tower,top} = \frac{m_{RNA} \cdot g}{A_{tower,top}} \propto m_{RNA}, A_{tower,top}^{-1} \tag{3.38}$$

where m_{rna} is the total mass off the RNA, g is the gravitational constant (9.81 m s^{-2}) and $A_{tower,top}$ is the cross-sectional area of the tower top. Equation (3.38) is used to scale the top diameter of the tower by keeping the stress constant, $\sigma_{tower,top,new} = \sigma_{tower,top,old}$. For this reason a new tower top cross-section is calculated to account for a change in RNA-mass, as shown in Equations (3.39) to (3.41).

$$\left(\frac{m_{RNA,new}}{m_{RNA,ref}}\right)\left(\frac{A_{tower,top,ref}}{A_{tower,top,new}}\right)\sigma_{tower,top,ref} = \sigma_{tower,top,ref} \tag{3.39}$$

$$\left(\frac{m_{RNA,new}}{m_{RNA,ref}}\right)\cdot\left(\frac{A_{tower,top,ref}}{A_{tower,top,new}}\right) = 1 \tag{3.40}$$

$$A_{tower,top,new} = \frac{m_{RNA,new}}{m_{RNA,ref}} \cdot A_{tower,top,ref} \tag{3.41}$$

For the tower top we again want to keep the ratio of wall thickness to outer diameter constant, in order to avoid buckling. Using the thin wall approximation for a hollow cylinder and Equation (3.33) for the wall thickness, we get Equation (3.42) which can be rewritten into Equation (3.43) to find a new outer diameter for the tower.

$$A_{tower,top,new} = 2 \cdot \pi \cdot D_{outer,new}^2 \cdot \Theta \tag{3.42}$$

$$D_{outer,new} = \sqrt{\frac{A_{tower,top,new}}{2 \cdot \pi \cdot \Theta}} \tag{3.43}$$

(3.44)

3.6.2.3. Top-to-Bottom Design

With the equations listed above the tower top and bottom are re-designed for their respective new loading conditions. The next step is to determine the dimensions of all the sections in between. This is done by applying a two scaling factors to each tower segment, which are weighted based on the height of the segment along the tower. For each tower segment i the new diameter $D_{new}(i)$ and wall thickness $T_{new}(i)$ can be determined using Equations (3.45) and (3.46):

$$D_{new}(i) = \left(z'(i) \cdot f_{top} + (1 - z'(i)) \cdot f_{bot}\right) D_{ref}(i) \tag{3.45}$$

$$t_{new}(i) = D_{new}(i) \cdot \theta(i) \tag{3.46}$$

where $z'(i)$ is the dimensionless height of the segment, f_{bot} is the scaling factor at the bottom of the turbine, f_{top} is the scaling factor at the top of the turbine, $D_{ref}(i)$ is the original diameter and $\theta(i)$ is the wall thickness ratio the tower segment i. The dimensionless height of the segment, $z'(i)$ is determined using Equation (3.47):

$$z'(i) = \frac{h(i)}{h_{tower}} \tag{3.47}$$

where $h(i)$ is the height of tower segment i and h_{tower} is the total height of the tower. The scaling factors f_{bot} and f_{top} are determined using Equations (3.48) and (3.49).

$$f_{bot} = \frac{D_{bot,new}}{D_{bot,old}} \tag{3.48}$$

$$f_{top} = \frac{D_{top,new}}{D_{top,old}} \tag{3.49}$$

3.6.3. Tower Mass and Cost

The scaled tower mass is calculated by calculating the mass of the individual tower sections and summing the result using Equation (3.50):

$$m_{tower} = \sum_{1}^{i} A_{tower,i} \cdot l_{tower,i} \cdot \rho_{tower} \tag{3.50}$$

where m_{tower} is the tower mass, and for each segment i $A_{tower,i}$ is the cross-sectional area, $l_{tower,i}$ is the tower segment length and ρ_{tower} is the mass density of the tower material. The amount of tower sections used is the same as the reference turbine. The mass density of the tower is calculated by taking the tower mass of the reference turbine and dividing that by the total volume of the tubular tower sections. This approach is taken to account for all the extra components that are inside the tower, such as stairs and safety equipment. The reference tower has a mass of 859.8 t (Gaertner et al., 2020b) and the volume is calculated to be 102.26 m^3, resulting in a tower density ρ_{tower} of 8408 kg m^{-3}. Using the new found mass, the cost of the tower can be calculated using Equation (3.51). The calculation is based on the WISDEM documentation of the NREL Cost and scaling model (NREL, 2019b), which gives a linear relation for the cost based on the tower mass. The same principle is applied for this calculation, re-calibrated on the IEA 15MW reference turbine, which has a mass of 859.8 tonnes and costs 4 028 245.91 $ (NREL, 2020; Gaertner et al., 2021), resulting in a specific cost of 4.67 $/kg, or 5.34 €/kg.

$$c_{tower} = 5.34 \cdot m_{tower} \tag{3.51}$$

3.6.4. Monopile Scaling

After the tower is scaled, the monopile has to be adjusted in order to fit the turbine tower. The monopile outer diameter is scaled to have the same diameter as the turbine tower base and will have the same diameter for its entire length. For each monopile segment, the ratio of outer diameter and wall thickness is kept constant to avoid buckling, in line with the scaling of the turbine tower. The new wall thickness is calculated using Equation (3.46). The embedment depth of the pile is kept constant with respect to the reference design. Scaling the monopile results in a change in monopile volume, which in turn results in a change in material and ultimately monopile costs. The mass of the monopile is calculated in the same way as the tower, using Equation (3.50). Using the new found mass, the cost of the monopile can be calculated using Equation (3.52). To calculate the cost of the new monopile, a linear relation for the cost based on the monopile mass is determined, using the available cost and mass figures of the IEA 15 MW reference turbine (Gaertner et al., 2020a). This reference monopile has a mass of 1076 tonnes and costs 2 780 390 $ (NREL, 2020; Gaertner et al., 2021), resulting in a specific costs of 2.58 $/kg, or 2.95 €/kg.

$$c_{monopile} = 2.95 \cdot m_{monopile} \tag{3.52}$$

3.6.5. Tower and Monopile Natural Frequency

After the tower and monopile are scaled, its natural frequency f_n is calculated, and it is checked whether it may result in an issue with the 1P and 3P blade passing frequencies. This is purely a check and, when it shows that issues arise, this will not instigate a re-design of the tower and monopile to overcome these issues. It is merely stated, to show whether the tower is valid or should require more attention. The natural frequency of the tower is determined by calculating the natural frequency of a stepped tower (Harlan et al., 1996). A schematic representation of such a stepped tower is shown in Figure 3.5.

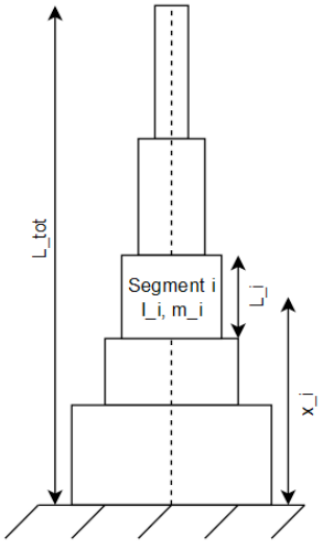

Figure 3.5: Schematic representation of a stepped tower (Harlan et al., 1996)

using the stepped tower model (Harlan et al., 1996), the natural frequency of the tower is calculated using Equations (3.53) to (3.57).

$$f_n = \left(\sqrt{\frac{4\pi^2 \left(m_{top} + m_{eq} L_{tot}\right) {L_{tot}}^3}{3EI_{eq}} \left(\frac{48}{\pi^4} + C_{found} \right)} \right)^{-1} \tag{3.53}$$

$$m_{eq} = \frac{\sum m_i l_i \left(1 - \cos \frac{\pi x_i}{2L_{tot}}\right)^2}{L_{tot}} \tag{3.54}$$

$$I_{eq} = \frac{\sum I_i l_i \cos^2 \frac{\pi x_i}{2L_{tot}}}{L_{tot}} \tag{3.55}$$

$$C_{found} = \frac{3EI_{eq}}{K_{eq} L_{tot}} \tag{3.56}$$

$$K_{eq} = \frac{K_R K_l L_{tot}^2}{K_R + K_l L_{tot}^2} \tag{3.57}$$

Where f_n is the tower natural frequency, m_{top} is the mass on top of the tower, m_{eq} is the tower equivalent mass described in Equation (3.54), L_{tot} is the tower length, I_{eq} is the tower equivalent moment of inertia described in Equation (3.55). C_{found} is a factor reflecting the influence of the flexibility of the foundation calculated with eq. (3.56) and K_{eq} is the foundation equivalent stiffness, where K_R is the rotational stiffness factor and K_L is the lateral translation stiffness factor. K_R and K_L are dependent on the soil type and are inputs by the user of the model. The effect of the foundation can also be omitted by setting $C_{found} = 0$, which is valid for very stiff foundations (Harlan et al., 1996). Since the soil conditions differ for every turbine location, the calculation of the natural frequency is simplified. The natural frequency of the tower and monopile assembly is calculated by setting L_{tot} to the length of the tower and monopile up to 4 times the monopile diameter beneath the seabed and assuming an infinitely stiff foundation there.

3.7. Total Turbine Cost

The sections above describe the scaling of mass and cost of the blades, generator and tower. However, a wind turbine consists of a multitude of other components. These components are not scaled in this study, but their costs are important to the total turbine cost. The mass values are used in the

tower scaling, described in Section 3.6. For this study, it is assumed that their mass and cost will be constant. The Low-Wind Turbine is based on the IEA 15 MW reference turbine, so all unchanging components will have the same values as the reference turbine (Gaertner et al., 2020a). Table 3.2 gives and overview of the turbine components and their respective mass, and the mass and cost of all the unchanging components combined. the total cost of all the unchanged components is calculated by taking the total cost of the turbine and substracting the original cost of the blades, generator and tower, as calculated by WISDEM for the IEA 15 MW RWT (NREL, 2020). WISDEM gives a total turbine cost of 18 107 973 $ (NREL, 2020; Gaertner et al., 2021), or 22 797 381 €.

Table 3.2: Overview of IEA WIND 15 MW reference turbine components with their respective mass and cost (Gaertner et al., 2020a; Gaertner et al., 2020b; NREL, 2020; Gaertner et al., 2021)

Component	**Mass [t]**	**Cost [k€]**
Blades	65.25 each	1077
Tower	859.8	4592
Monopile Foundation	1076	3170
Generator	371.6	2723
Hub mass	190	-
Nose Cone	11.39	-
Bedplate	70.329	-
Low Speed Shaft	15.734	-
Shaft Bearing (SRB)	5.664	-
Shaft Bearing (TDO)	2.23	-
Flange	3.964	-
Yaw System	100	-
other (electronics, thermal, etc.)	50	-
Total of Other Components	**449**	**9081**
Total	**2951**	**22797**

Combining all the information from the sections above, an equation for the total cost of the scaled turbine can now be determined. The total turbine cost $c_{turbine}$ is calculated using Equation (3.58):

$$c_{turbine} = 9081103 + 3 \cdot c_{blade} + c_{generator} + c_{tower} + c_{monopile} \tag{3.58}$$

Where 9 081 103 € is the sum of the unchanged components of the turbine, c_{blade} is the cost of one blade which is multiplied by 3 for the total number of blades, $c_{generator}$ is the cost of the direct drive generator, c_{tower} is the cost of the tower and $c_{monopile}$ is the cost of the monopile.

4

Model Inputs

This chapter presents the inputs for the simulations, performed using the model developed for this thesis. The goal of this chapter is to provide an overview of the used input data and their sources. Section 4.1 explains how all cost figures are converted to 2020 Euros. Section 4.2 presents the characteristics of the two reference turbines used in this study. The two reference turbines used in this thesis are the 3.4 MW land-based wind turbine, and the 15 MW offshore wind turbine, both developed for the International Energy Agency (IEA). Section 4.3 presents the parameters used for the modelling of the offshore and onshore wind farms. For the offshore wind farms, the subsections cover the losses, available area, component costs, installation costs and operation and maintenance costs. For the onshore wind farms, the subsections cover only the losses and installed capacities. Since the onshore wind farms of the power model remain constant for all simulation, their costs are not considered. Section 4.4 presents the efficiencies of the different components of a PV system that are used in this thesis, also without consideration of costs. Section 4.5 describes the cost and characteristics of the storage types that have been modelled in this thesis.

4.1. Converting monetary values

The information used in this thesis is not all from the same time period. Also, different sources of information may use different currencies, such as Euros, US Dollars and British pounds. In order to be able to compare and use cost figures throughout this thesis, all used data is expressed as 2020 Euros. Monetary cost figures in US Dollars from past years are converted to 2020 US Dollars with the help of an online inflation calculator (Westegg, 2021), which uses the Consumer Price Index to correct the values. To convert 2020 US Dollars to Euros a conversion rate of 1.14 €/$ is used, while the conversion for GBP to euros is 1.12 €/£ (Exchangerates.org.uk, 2021).

4.2. Turbines

This section present the data of the reference turbines that have been used in the model of this thesis. Section 4.2.1 presents the offshore turbine used in the power model, and which also serves as the starting point for the Low-Wind cost and scaling model. Section 4.2.2 presents the land-based turbine that is used in the power model.

4.2.1. Offshore Turbine

For the offshore wind turbine this thesis uses the IEA 15 MW reference turbine(Gaertner et al., 2020a). Table 4.1 gives an overview of the offshore turbine characteristics essential for the power model of this study. In Chapter 5, Table 5.1 and Figure 5.2 give a more comprehensive overview of the turbine. Figure 4.1 shows the power curve of the offshore turbine. The offshore turbine serves two purposes in this thesis. First, it serves as the reference design to base the Low-Wind turbine off of. This turbine is chosen for this purporse, as it is the reference turbine with the largest rotor and rated power currently available. This makes it a suitable starting point for the Low-Wind turbine, because this turbine concept requires a large rotor diameter in order to still have a reasonable rated and specific power. Secondly,

this turbine serves the role of the conventional turbine in the model. The current trend for offshore wind turbines is to have increasingly large rotors and power ratings. Currently, the GE Haliade-X is the largest commercially available wind turbine, with a rotor diameter of 220 m and a rated power of 14 MW (General Electric, 2021). Assuming this trend continues, and with the fact that the IEA 15MW is considered a feasible reference design, the IEA 15 MW reference turbine is chosen as the conventional turbine.

Table 4.1: IEA 15 MW reference turbine data, adapted from (Pietro Bortolotti et al., 2019)

Data	Value
Rated electrical power	15 MW
Maximum c_p	0.481
Efficiency	93 %
Hub height	150 m
Rotor Diameter	240 m
Cut-in wind speed	3 m s^{-1}
Rated wind speed	10.58 m s^{-1}
Cut-out wind speed	25 m s^{-1}

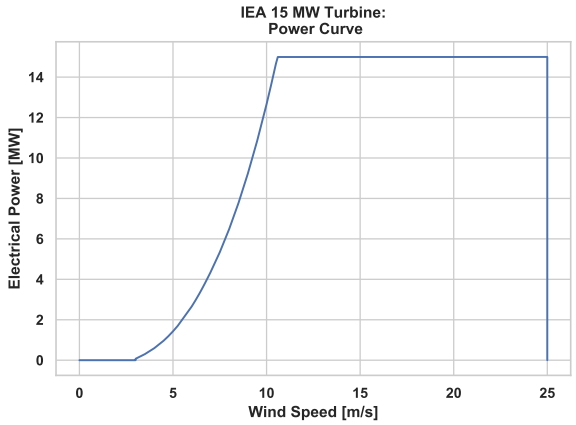

Figure 4.1: IEA 15 MW Reference Turbine Power Curve

4.2.2. Onshore Turbine

The reference turbine that will be installed onshore is the IEA 3.4 MW reference turbine (Pietro Bortolotti et al., 2019). This reference turbine has been developed especially for onshore applications. Table 4.2 gives an overview of the turbine characteristics essential to this study. Only data needed for the calculation of the aerodynamic power output of the turbine is presented. The power curve of the IEA 3.4 MW reference turbine is shown in Figure 4.2.

4.3. Wind Farms

This section presents the parameters used for the power model and cost calculations in this thesis. Section 4.3.1 presents the losses that have been modeled for the onshore and offshore wind farms. **??** presents the installed capacity for the onshore turbines for each of the Dutch provinces. Section 4.3.3 presents the location and available area for each of the modelled offshore wind farms. Section 4.3.4 presents the components cost parameters for the BOP of the windfarms. Section 4.3.5 presents the cost figures used for the installation of the offshore wind farms. Section 4.3.6 presents the operations and maintenace (O&M) costs for the offshore wind farms

Table 4.2: IEA 3.4 MW reference turbine data, adapted from (Pietro Bortolotti et al., 2019)

Data	Value
Rated electrical power	3.37 MW
Maximum c_p	0.481
Efficiency	93.6 %
Hub height	110 m
Rotor Diameter	130 m
Cut-in wind speed	4 m s^{-1}
Rated wind speed	98 m s^{-1}
Cut-out wind speed	25 m s^{-1}

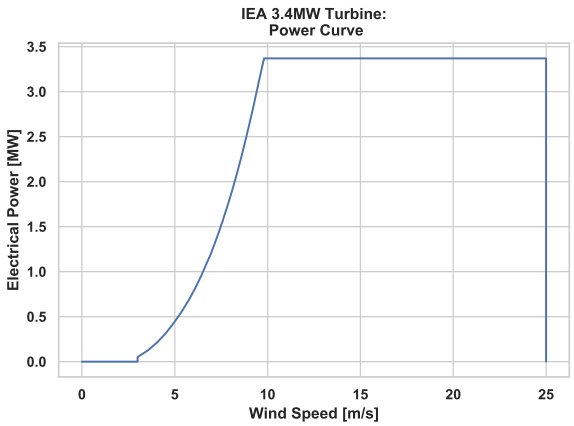

Figure 4.2: IEA 3.4 MW Reference Turbine Power Curve

4.3.1. Wind Farm Losses

The Wind farm losses implemented in the model are wake losses, transportation losses and availability of the wind turbines in the wind farm. The values used for these losses are tabulated in Table 4.3. For the onshore wind farms no transportation losses are taken into consideration, as they are already close to the demand. The spacing of the wind turbines in the wind farm will be fixed at 5 D × 10 D arrays for all wind farms, resulting in an array power loss of around 10 percent (Manwell et al., 2002). This study uses a transportation loss of 6.7×10^{-3} % km^{-1} (Ardelean et al., 2015). The wind turbine availability factor is based on the portfolio 2018–19 from the System Performance, Availability and Reliability Trend Analysis (SPARTA) platform (SPARTA, 2021). SPARTA states an average Production Based Availability (PBA) of 95 %. The availability can also be interpreted as loss of 5 % of total wind farm power, since this portion of the wind turbines is unavailable.

Table 4.3: Wind farm loss percentages (Manwell et al., 2002; Ardelean et al., 2015; SPARTA, 2021)

Loss	Value[%]	Source
Wake losses	10	(Ardelean et al., 2015)
AC transportation losses	6.7×10^{-3} km^{-1}	(Manwell et al., 2002)
Turbine unavailability	5	(SPARTA, 2021)

4.3.2. Onshore: Installed Capacity

The installed power is divided over the different provinces as shown in Table 4.4, which represent all known turbines already installed and in development as of 2019 (Rijksdienst voor Ondernemend Nederland, 2020). This study assumes that all currently known projects will be completed. The model simulates a single wind park for every province. Each windpark is filled with the land-based wind

turbines, until it meets the capacity for that province.

Table 4.4: Overview of modelled installed capacity per province (Rijksdienst voor Ondernemend Nederland, 2020)

Province	**Installed capacity [**MW**]**
Flevoland	1871.3
Groningen	971.9
Zuid-Holland	976
Noord-Holland	698
Zeeland	638.8
Friesland	620.3
Noord-Brabandt	654.4
Drenthe	316.5
Gelderland	339.8
Limburg	134.1
Overijssel	88.8
Utrecht	79.1
Total installed onshore	7389

4.3.3. Offshore: Available Area

Table 4.5 tabulates the data for the different offshore wind farm locations. All of these locations, except Dogger Bank, are currently existing wind farms or planned locations, to be constructed within the near future. Dogger Bank is located in the North-West corner of the EEZ, shown in Figure 2.4. Tennet, the Dutch TSO has presented plans for the construction of a artificial island and large wind farms on the Dogger Bank. For this reason, the Dogger Bank has been added as a location in this study. Assuming that 10 % of the available area will still be in use for oil and gas industries, this leaves and available area of 4161 km^2 for wind turbines (Royal Haskoning DHV, 2017). It is assumed that all these locations can be fully utilised for the installation of offshore wind farms. The spacing of 5 D $\times$ 10 D, mentioned in Section 4.3.1 is also used to determine the amount of turbines that can be installed within the available area. This results in a total area of 6816 km^2.

Table 4.5: Overview of offshore wind farms with their available area and locations (Wikipedia, 2021; Royal Haskoning DHV, 2017)

Name	**Area [**km^2**]**	**Latitude [**°**]**	**Longitude [**°**]**	**Source**
Borssele	344	51.583	3.0	(Wikipedia, 2021)
Dogger Bank	4161	55.415	3.786	(Royal Haskoning DHV, 2017)
Gemini	68	54.036	5.963	(Wikipedia, 2021)
Hollandse Kust Zuid	236	52.367	4.117	(Wikipedia, 2021)
Hollandse Kust Noord	173	52.589	4.206	(Wikipedia, 2021)
Hollandse Kust West	176	52.640	3.790	(Wikipedia, 2021)
Hollandse Kust Noordwest	190	52.940	4.081	(Wikipedia, 2021)
Hollandse Kust Zuidwest	232	52.376	3.798	(Wikipedia, 2021)
IJmuiden Ver	1170	52.839	3.644	(Wikipedia, 2021)
Luchterduinen	25	52.417	4.167	(Wikipedia, 2021)
NoordzeeWind	27	52.606	4.419	(Wikipedia, 2021)
Prinses Amalia Windpark	14	52.589	4.206	(Wikipedia, 2021)
Total area	6816			

4.3.4. Offshore: Component Costs

The cost figures for the BOP components are derived from a BVG Associates report (BVG Associates, 2019). The cost of these components are stated in Table 4.6. The first three columns present the data

extracted from the report, while the fourth column presents the cost figures used in the model.

Table 4.6: Overview of offshore 1 GW wind farm components costs, adapted from (BVG Associates, 2019)

Component	**Units**	**Total Cost [**M€**]**	**Unit Cost [**M€**]**
Export cables	60 km, 1 GW	146	2.4×10^{-3} km^{-1} MW^{-1}
Array cables	100 km, 1 GW	39	0.4×10^{-3} km^{-1} MW^{-1}
Offshore substation	3	134.4	45 per substation (500 MW)
Onshore substation	1	34	34 per substation
Operations base	1	9	9 per base

4.3.5. Offshore: Installation Cost

For the installation cost of an offshore wind turbine we again look at the BVG Associates report (BVG Associates, 2019). For a 1 GW offshore wind farm, consisting of 100 10 MW wind turbines, they estimate the total installation and commissioning cost at 650×10^6 £, or 728×10^6 €. A breakdown of the wind farm installation costs, as presented in the BVG Associates report, is shown in Table 4.7. The first three columns present the data extracted from the report, while the fourth column presents the cost figures used in the model.

Table 4.7: Overview of offshore 1 GW wind farm installation costs, adapted from (BVG Associates, 2019)

Activity	**Units**	**Total Cost [**M€**]**	**Unit Costs [**M€**]**
Foundation installation	103	112	1.1 per foundation
Offshore substation installation	3	39	13 per substation
Onshore substation installation	1	28	28 per substation
Onshore export cable installation	-	5.6	5.6 per wind farm
Offshore cable installation	160 km	246	1.5 km^{-1}
Turbine installation	100	56	0.6 per turbine
Offshore logistics	-	4	4 per wind farm
Other (Insurance, Contingency, etc.)	1 GW	237	237×10^{-3} MW^{-1}

4.3.6. Offshore: Operation and Maintenance Costs

The operation and maintenance cost figures are based on the BVG associates paper (BVG Associates, 2019) and shown in Table 4.8. The cost figures are expressed per turbine and per year, so they can be used for every wind farm in the system. It is assumed that O&M costs are dominated by logistics, staff and equipment that does not differen between Low-Wind turbines and conventional turbines. Therefore, this thesis assumes the same O&M costs for both the conventional and Low-Wind turbine.

Table 4.8: Operations, Maintenance and Decommissioning costs (BVG Associates, 2019)

Type	**Units**	**total cost[**M€**]**	**cost per unit[**M€**]**
Operations	100	84	8.4 yr^{-1}
Maintenance	100	56	0.6 yr^{-1}

4.4. Solar Farms

Table 4.9 presents the components of the PV systems considered for this study, and their respective efficiencies. The main active components of a PV system are the modules, inverters and the cables connecting them. Crystalline silicon solar (c-Si) modules are used, since they are currently the most widely adapted and matured technology. Since the focus of this study is not solar energy, a simple

approach is taken with a fixed value for the total lumped system efficiency. c-Si modules generally have a module efficiency of around 18 % (Smets et al., 2016). Inverters convert the DC power coming from the PV array and generally have an efficiency of 95 % (Laboratories, 2021). The study assumes low losses in the cables and other losses, resulting in an efficiency of 99 %. This brings the total solar-to-electricity efficiency to 16.75 %.

Table 4.9: Overview of Main PV system components, their respective efficiencies and total system efficiency (Smets et al., 2016; Laboratories, 2021)

Component	**Efficiency [%]**	**Source**
Modules	18	(Smets et al., 2016)
Inverter	95	(Laboratories, 2021)
Ohmic	99	
Other	99	
Total system efficiency	16.75	

4.5. Storage

The storage types which are considered in this study are: Vanadium Redox-Flow batteries (VRFB), Compressed Air Energy Storage (CAES) ans Lithium-ion batteries. The chosen storage types are all considered mature technologies and have sufficient technical and cost-data available. Different technologies are chosen to create insight in their cost-effectiveness for large scale energy storage. Also, these technologies do not rely on external conditions such as elevation differences, meaning they can be placed within The Netherlands. Table 4.10 presents an overview of the performance and cost characteristics of the different storage technologies. For each storage technology the maximum noted efficiency is taken, as future technological improvements will result in fewer losses. For each technology the lowest price is selected, assuming that when buying large quantities a low price can be offered. Also, future advancements in the storage technologies can drive their respective prices down. The O&M costs of the technologies are a percentage of the storage CAPEX, and are yearly costs.

Table 4.10: Storage cost and performance characteristics, adapted from (Baxter, 2019)

	Unit	**VRFB**	**CAES**	**Lithium**
Cost		360 €/kWh	1905 €/kW	475 €/kWh
Lifespan	yr	20	40	10
Efficiency (AC-AC)	%	80	80	90
Depth of Discharge	%	100	100	80
Degradation	%	0	0	2
O&M	% yr^{-1}	3	1	2

5

Results & Discussion

This chapter presents, describes and discusses the main results from the models created for this thesis. Section 5.1 presents and discusses the re-designed Low-Wind Turbine and compares it to the original 15 MW IEA Reference Turbine. Section 5.2 presents and discusses the data from the inital simulations that were done with the power model. Section 5.3 presents and discusses the results of the sensitivity analysis performed.

5.1. Low-Wind Turbine Scaling

The Low-Wind turbine has been designed by applying scaling relations, described in Chapter 3, to the IEA 15MW reference turbine. The following sections present the results of this model and compare them to the original reference turbine, in order to assess the changes. The results are accompanied by a description of the changes and an assessment of the feasibility of the new design. Results which might lead to problems in the design do not institute a re-design, but indicate that these components should be reconsidered. This in turn implies that the cost of that component is not accurate. Section 5.1.1 presents and discusses the changes of the main parameters between the Low-Wind and the reference turbines. Section 5.1.2 gives a graphical representation of the changes in geometry of the blades, tower and monopile. Possible issues with the natural frequency of the support structure are also assessed, using a campbell diagram. Section 5.1.3 presents and discusses the change in cost of the scaled components and the resulting cost of the Low-Wind turbine.

5.1.1. Turbine Parameters

This section presents and assesses the main parameters of the Low-Wind turbine. Table 5.1 gives an overview of the most important parameters of the IEA 15 MW and the Low-Wind turbines, in order to show the changes. The last column of the table shows the change relative to the original reference turbine, in percentages. The Low-Wind turbine main design driver is the lower rated wind speed of only $7\,\mathrm{m\,s^{-1}}$. This drastically lowered wind speed reduces the maximum loading situation on the turbine components, which in turn gives room in the design to decrease the amount of material used for the blades, generator, tower and monopile. This reduction in used material leads to reduction in total mass of 35 %, from 2951 t to 1913 t for the total turbine. Reducing the amount of material used is the main goal of the model, as the costs of the individual components are a direct result of its mass, except for the generator. Overall it can be concluded that the scaling model had the desired result in reducing the mass of the individual components, and thereby the total cost of the Low-Wind Turbine. Figure 5.1 shows the power curve of the newly designed Low- Wind turbine. The Low-Wind turbine has a rated wind speed $7\,\mathrm{m\,s^{-1}}$, and a cut-out wind speed of $15\,\mathrm{m\,s^{-1}}$.

5.1.2. Blades, Tower, Monopile

This section presents the geometric properties of the blade, tower and monopile of the Low-Wind and IEA 15MW turbine, which can be seen in Figure 5.2. Also, issues between the natural frequency of the Low-Wind tower and the 1P and 3P harmonics are assessed.

Table 5.1: Comparison between IEA 15 MW and Low-wind Turbine Technical Specifications

Parameter	Units	IEA 15MW	Low-Wind Turbine	Change [%]
Power rating	MW	15	4.33	-71
Specific rating	$W\,m^{-2}$	332	96	-71
Number of blades	-	3	3	
Cut-in wind speed	$m\,s^{-1}$	3	3	
Rated wind speed	$m\,s^{-1}$	10.59	7	-34
Cut-out wind speed	$m\,s^{-1}$	25	15	-40
Rotor diameter	m	240	240	
Design tip speed ratio	-	9.0	9.98	11
Minimum rotor speed	RPM	5.0	3.61	-28
Maximum rotor speed	RPM	7.56	5.56	-26
Maximum tip speed	$m\,s^{-1}$	95	69.86	-26
Blade mass	t	65	40.5	-38
Generator mass	t	371.6	146	-61
RNA mass	t	1017	717	-29
Tower mass	t	859.9	542	-37
Tower top diameter	m	6.5	5.46	-16
Tower base diameter	m	10	7.59	-24
Monopile base diameter	m	10	7.59	-24
Monopile mass	t	1076	655	-39
Tower-monopile natural frequency	Hz	0.18	0.13	-27

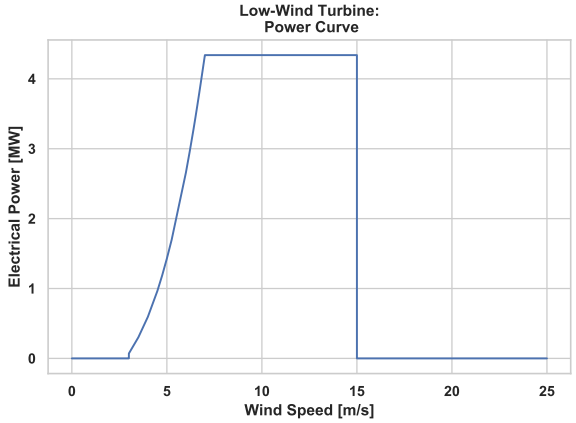

Figure 5.1: Low-Wind Turbine Power Curve

Figure 5.2a shows the chord distributions along the non-dimensional span of the blades of the IEA 15 MW and the Low-Wind turbine. The figure shows that the chord of the Low-Wind blade is more slender than the reference blade. The more slender chord is enabled by the increase in TSR, from 9 tot 9,98. This increase in TSR fully utilises all the headroom in the loading situation that was made available because of the reduction in rated wind speed, as described in Section 3.4. Again, the main goal was to reduce the blade mass, as this results in a reduction in costs. Figure 5.2b shows the twist distributions along the non-dimensional span of the blades of the IEA 15 MW and the Low-Wind turbine. The twist of the blade is adjusted in order to keep the airfoils operating at their optimal angle of attack,

compensating for the increased TSR.

Figure 5.2c shows the outer diameter versus elevation for the tower and monopile combined. The transition between the tower and the monopile occurs at an elevation of 15 m, presented by the highest of the dashed horizontal lines. The upper diameter of the Low-Wind tower is reduced to 5.46 m as a result of the reduction in RNA mass. The bottom diameter of the Low-Wind tower is reduced to 7.59 m as a result of the reduction in moment caused by the thrust force. The scaling of all the segments between the top and bottom is decribed in Section 3.6.2. Looking at the gradient of the Low-Wind tower outer diameter, it can be seen that for the bottom segments of the tower the diameter increases when compared to the segments below, instead of remaining constant or decreasing. This is a direct results of the modelling approach, and can be explained when looking at the reference outer diameter, f_{bot} and f_{top}, from Equations (3.48) and (3.49). For this particular design, $f_{bot} = 0.759$ and $f_{top} = 0.84$. Filling in these values in Equation (3.45), it can be seen that for a certain increase in the dimensionless height $z'(i)$, f_{top} contributes more to the ultimate factor than f_{bot} does. Combining this with a reference tower with several segments where the outer diameter is nearly constant, the result is an increased diameter for higher tower segments. The same applies to the tower and monopile wall thickness, as can be seen in Figure 5.2d. These flaws are worth noting and should be considered more thoroughly when refining the design of the Low-Wind turbine. However, for the goal of this study this is not of great importance and therefore considered passable.

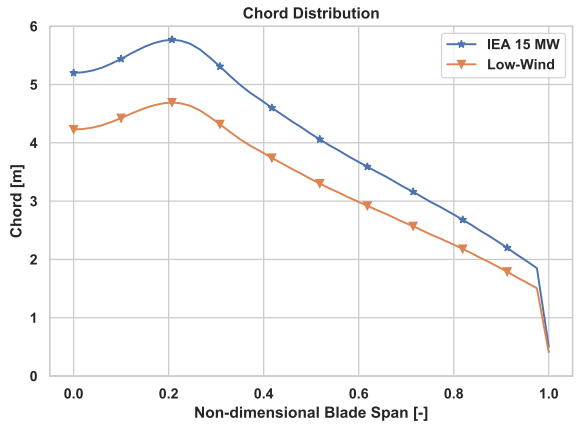

(a) Blade Chord Distributions of the IEA 15 MW and Low-Wind Turbines

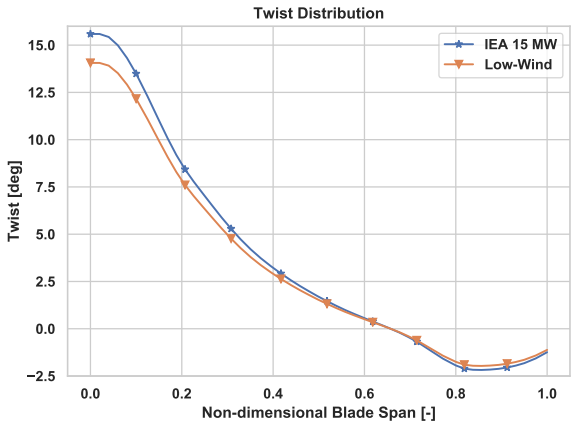

(b) Blade Twist Distributions of the IEA 15 MW and Low-Wind Turbines

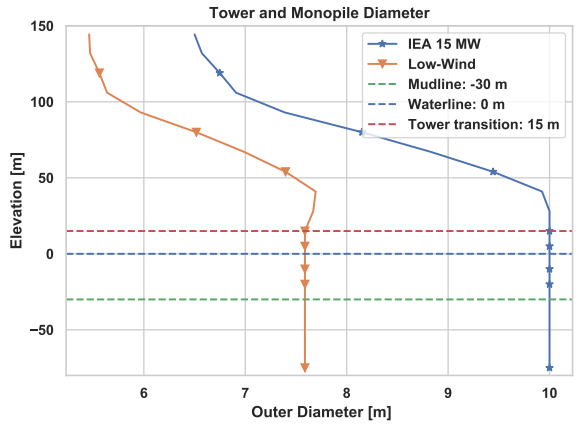

(c) Tower and Monopile Diameter of the IEA 15 MW and Low-Wind Turbines

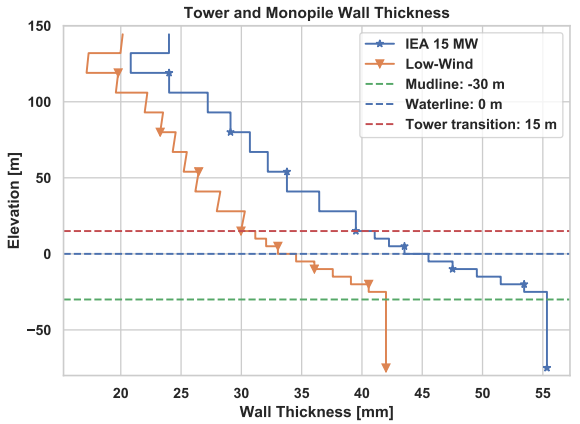

(d) Tower and Monopile Wall Thickness of the IEA 15 MW and Low-Wind Turbines

Figure 5.2: Graphical representations of IEA 15 MW and Low-Wind Turbines, showing differences in blade chord, blade twist and tower outer diameter and wall thickness

Figure 5.3 shows the campbell diagram of the Low-wind turbine, in order to assess if there might be issues between the 1P, 3P frequencies and the Low-Wind tower natural frequency. The Low-Wind turbine has a tower natural frequency of 0.13 Hz, compared to 0.18 Hz for the reference tower. Because

of the reduction of the minimum and maximum rotational speed of the rotor, the tower remains a soft-stiff design with enough margin between the tower natural frequency and the 1P and 3P harmonics. However, it should be noted that the North Sea has an average wave period of 5 to 7 seconds (Lavidas et al., 2019), meaning the upper end of the spectrum, at 0.12 Hz, comes close to the natural frequency of the tower. The effect this has on the loading situation of the tower is not discussed further in this thesis, but might mean that both the tower and monopile need a new design. This in turn results in a different cost of the tower and monopile. However, the resulting tower and monopile cost are taken as-is for further cost calculations.

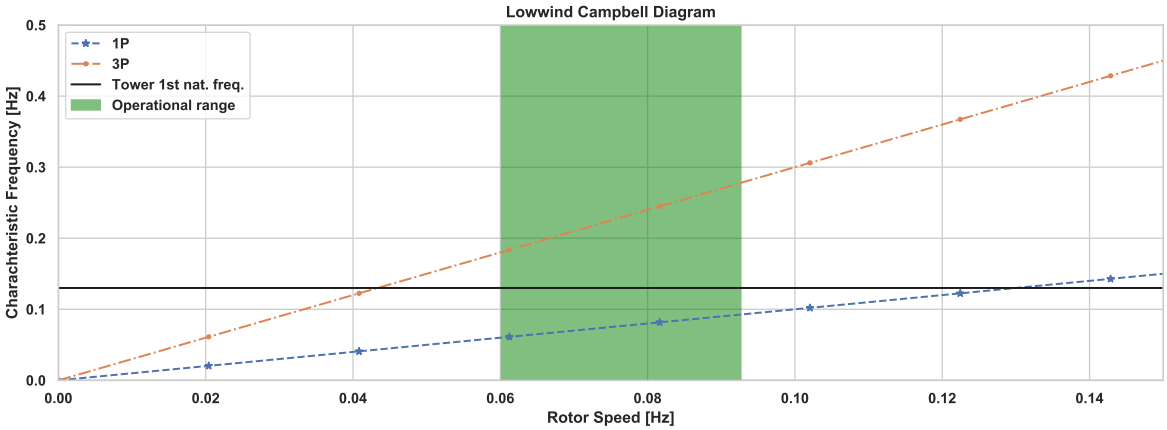

Figure 5.3: Low-Wind Turbine Campbell Diagram

5.1.3. Low-wind turbine Costs

Table 5.2 presents the cost of the components of the Low-Wind turbine. All scaled components show a significant cost reduction, enabled by the lower loading situation. Ultimately, the Low-Wind turbine scaling model achieves a total cost reduction of 26.2 %. The calculation methods for the costs of the individual components are all based on simple mass and cost scaling relations and might therefore not be very accurate. Especially the calculation of generator cost, which now is 60.9 % cheaper compared to the reference design, might need a more detailed calculation method. The calculation of the generator cost might be inaccurate, since its cost solely depends on the power rating of the turbine and do not account for generator torque. The effect the cost-inaccuracy of the Low-Wind turbine has on the total system costs is assessed by performing a sensitivity analysis on this cost figure, of which the results are shown in Section 5.3.1.

Table 5.2: Low-Wind Turbine Cost Breakdown

Component	**Cost [k€]**	**Change [%]**
Blade	619	−42.5
Generator	1063	−60.9
Tower	2894	−37.0
Monopile	1933	−39.0
Rest	9081	0
Total	16830	−26.2

5.2. Power Model Simulation Results

The following sections present the data generated by the model. The datasets for each storage technology are obtained by running the model over a range of settings for the amount of conventional and Low-Wind turbine. For each simulation the model calculates the required storage capacity and its cost, as well as the cost of the onshore wind farms. The settings for the turbines range from 100 to

8000 conventional turbines and 0 to 8000 Low-Wind turbines, with a stepsize between simulations of 100. The sum of conventional and Low-Wind turbines never exceeds 8000, as this is the maximum amount that can be placed within the available offshore areas. This range of simulation is performed three times, with different storage technologies. The selected storage technologies are VRFB, CAES and Lithium-ion batteries, because of their individual characteristics. The goal of these simulations is to create insight into the effect that Low-Wind turbines have on the capacity of the respective storage technology and ultimately the total system cost. Throughout the sections below and next chapters, the term system costs refers to the combined yearly cost of the offshore wind farms and required storage. Section 5.2.1 presents the effect Low-Wind turbines have on the annual energy production. Sections 5.2.2, 5.2.3 and 5.2.4 present the results of the model when using VRFB, CAES or Lithium-ion storage technologies, respectively.

5.2.1. Overplanting Factor

Figure 5.4 shows the effect of Low-Wind turbines on the total yearly energy production. This figure is only presented once, as it is identical for all storage technologies. The overplanting factor is determined by dividing the total yearly produced energy from offshore wind, onshore wind and solar by the total demand. The heatmap show two diagonal borders on the left-hand side and the right-hand side. The left-hand side diagonal border corresponds with the simulations where the overplanting factors is higher than 1 and $SOC(t = 0) \leq SOC(t = T_{end})$. The right-hand side diagonal borders corresponds with the simulations where the maximum amount of offshore turbines that can be placed in the given area is reached. All simulations along this border contain the same amount of turbines; since the area-use per turbine is a function of rotor diameter, both Low-Wind and conventional turbines require the same amount of space. The Low-Wind turbines contribute less to the overplanting factor than the conventional turbine do. This is expected, as both their rated and cut-out wind speed are lower, harvesting less of the available wind. However, the goal of the Low-Wind turbines is not to compete directly with conventional multi-MW turbines, but rather provide a cost-effective alternative, reducing total system cost.

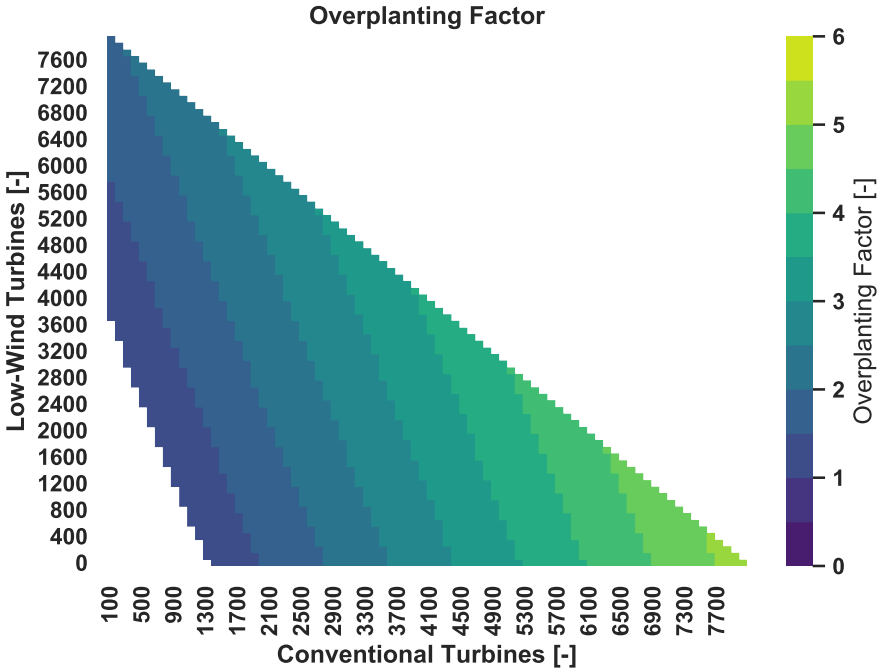

Figure 5.4: Overplanting Factor for Different Amounts of Conventional and Low-Wind Turbines

5.2.2. Vanadium Redox Flow Batteries

This section presents and discusses the results from the model simulations, when using VRFB as storage technology. The graphs shown in this section are also shown for the simulations with CAES and Lithium as a storage technology. Figure 5.5a shows a heatmap of the calculated storage capacities for all simulations. Figure 5.5b shows a heatmap of the total system cost for each of the simulations. The colorbars of the heatmaps have a logarithmic scale. On both heatmaps, horizontal and vertical dashed lines are plotted. The location of the intersection of the two lines corresponds with the simulation with minimum costs. The dashed lines occur at the same location for both heatmaps. The lines themselves represent cross-sections through the heatmap, which are presented and discussed later in this section. The simulations with minimum and maximum storage capacities and costs are tabulated in Table 5.3, along with their important parameters.

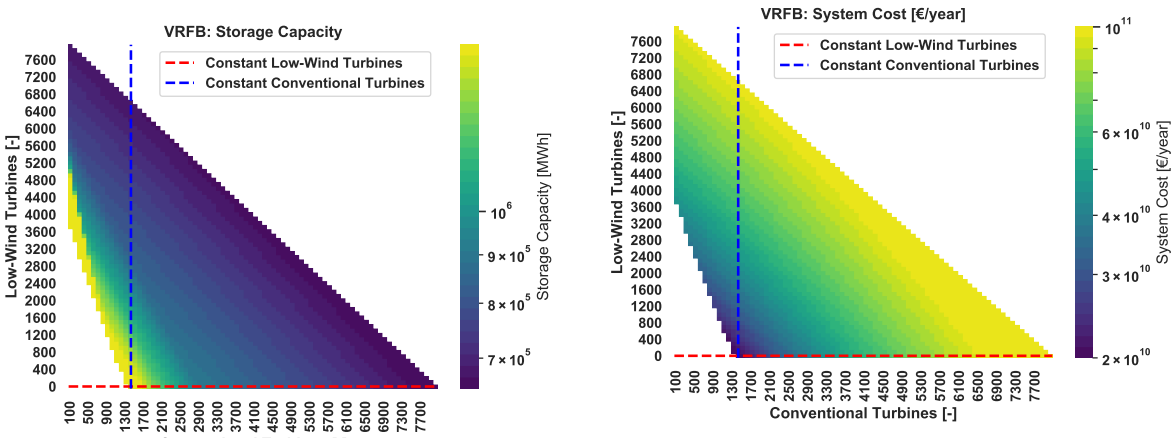

(a) VRFB Storage Capacities for Different Amounts of Conventional and Low-Wind Turbines

(b) VRFB: Total System Costs for Different Amounts of Conventional and Low-Wind Turbines

Figure 5.5: VRFB: Heatmaps of storage capacity and system cost for all simulations using VRFB as storage technology

Table 5.3: Minimum and Maximum values for all simulations using VRFB Storage technology

	Unit	Minimum Storage Capacity	Minimum System Cost	Maximum Storage Capacity	Maximum System Cost
Conventional Turbines	turbines	8000	1400	100	8000
Lowwind Turbines	turbines	0	0	3700	0
Overplanting Factor	-	5.20	1.16	1.09	5.20
Storage Capacity	10^6 MW h	0.6467	1.878	7.923	0.6467
Import	MW h	1452	1600	3549	1452
Export	10^6 MW h	39.862	3.647	0	39.862
Wind Cost	10^{10} €/yr	12.01	1.881	4.5415	12.01
Storage Cost	10^{10} €/yr	0.0023	0.0067	0.0283	0.0023
System Cost	10^{10} €/yr	12.01	1.887	4.5437	12.01

Looking at Figure 5.5a, it can be seen that the lowest storage capacities are achieved on the right diagonal border of the heatmap. All points along this border represent a simulation where all the available offshore locations have been filled to the maximum possible. This is expected, as overplanting increases the produced power at every time step, reducing the amount of mismatch and thereby the needed storage capacity. The simulation with the lowest storage capacity occurs at 8000 conventional and 0 Low-Wind turbines. The respective simulation has a overplanting factor of 5.2. However, high overplanting factors can only be achieved by installing a large amount of turbines, incurring significant capital and maintenance costs. Since not all excess energy in the system can be exported and has to be curtailed, these costs are essentially wasted. Because of this, the same simulation is also the

simulation with maximum system costs. Figure 5.5b shows a minimum total system cost at the lower border of the heatmap. The points along this border represent simulations where no Low-Wind Turbines have been installed. The simulation with the lowest system cost occurs at 1400 conventional and 0 Low-Wind Turbines. This simulation has an overplanting factor of 1.16, and has the minimal amount of turbines required to satisfy all constraints. The other simulation that satisfies all constraints is for 1300 conventional turbines and 100 Low-Wind turbines, which has a storage capacity of 2.477×10^6 MW h and a system cost of 1.889×10^{10} €/yr. In the case of the second simulation, the cost reduction achieved by the installation of 100 less expensive Low-Wind turbines are negated by the cost incurred from the increased storage capacity.

It should also be noted that the found minimal and maximal solutions are a result of the chosen turbine step size between simulations. When choosing a step size between simulations of single turbines, the simulation with the exact amount of turbines that would result in minimal system costs can be found. However, this thesis aims to show the general patterns and relations between storage and wind costs, and the exact optimum is therefore beyond the scope of this thesis. The chosen step size of 100 turbines is deemed sufficient to show the desired results.

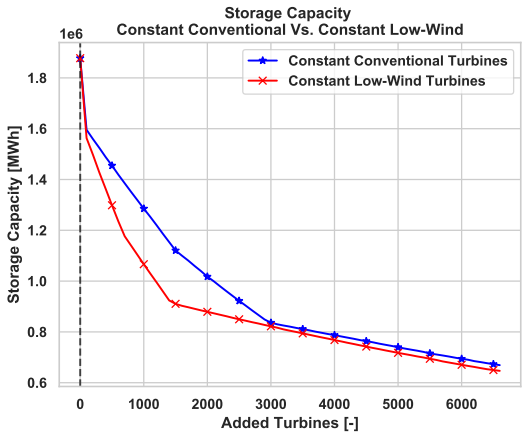

(a) VRFB: Storage capacity graphs for constant Conventional and constant Low-Wind turbines

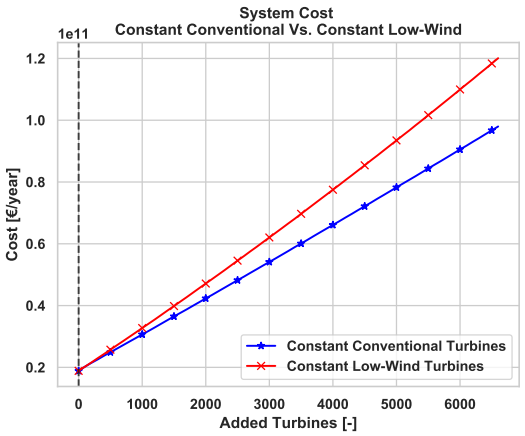

(b) VRFB: System cost graphs for constant Conventional and constant Low-Wind turbines

Figure 5.6: VRFB: Cross-sections through heatmaps, showing trends in storage capacity and system cost for constant conventional and constant Low-Wind turbines

Figures 5.6a and 5.6b show the horizontal and vertical cross-sections of the storage capacity and system cost heatmaps shown above. Since the minimum cost solution lies on the border of the heatmap, subtracting turbines is not possible. The horizontal cross-section shows the trends in storage capacity and total system cost when adding conventional turbines at constant Low-Wind turbines, while the vertical cross-section shows the trends when adding Low-Wind turbines at constant conventional turbines. As the simulation with minimum costs lies on the border of the heatmap, the amount of conventional and Low-Wind turbines can not be decreased. Figure 5.6a shows that, when close to the minimum system cost simulation, adding turbines to the system has a significant impact on the required storage capacity. From 0 to around 100 additional turbines, the effect of both conventional and Low-WInd turbines is similar. From 100 to 3000 additional turbines, adding conventional turbines has a greater effect on the reduction of the required storage capacity than Low-Wind turbines. After about 3000 turbines the effect becomes similar again.

It can also be seen that both storage capacity lines are composed of several linear segments with different slopes. There can be several explanations for this behaviour. One explanation can be that these kinks are the results of a certain constraint being satisfied and another one becomes normative. Another explanation can be that another point in the time series becomes normative. The exact reason behind this behaviour is beyond the scope of this thesis. Figure 5.6b shows that adding conventional turbines is slightly more expensive than Low-Wind turbines. The increase in total system cost seems to show a nearly linear pattern. Although adding Low-Wind turbines is slightly less expensive than conventional turbines, between 100 and 3000 added turbines their effect on the reduction of storage capacity is also much less. For instance, at a storage capacity of 1×10^6 MW h, around 1200 extra

conventional turbines are needed, resulting in a system cost of 0.3×10^{11} €, while 2200 extra Low-Wind turbines are needed, which results in a system cost of more than 0.4×10^{11} €. Only for large reductions of storage capacities, when high overplanting is needed, can Low-Wind turbines provide a cost-effective solution.

From the information provided by the storage capacity heatmap, it can be concluded that Low-Wind turbines do not contribute to the minimisation of storage capacity, since the simulation with minimum storage cost does not contain Low-Wind turbines. The system capacity heatmap shows that Low-Wind turbines also do not contribute to minimising total system costs, since the minimum cost simulation also does not contain Low-Wind turbines. In the situation where the storage capacity at minimum system costs is not feasible, more wind generation has to be installed to lower this capacity. When looking at the horizontal and vertical cross-sections, it can also be concluded that Low-Wind turbines do not provide a cost-effective alternative for reducing the total storage capacity. Only when the required storage amount has to be lowered by a significant amount can Low-Wind turbines compete with conventional turbines. For these settings, wind costs dominate the systems cost, and therefore the simulation with minimal costs appears at the bottom left corner of the heatmap, where the least amount of turbines are installed.

5.2.3. Compressed Air Energy Storage

This section presents the outcome of the model, when using CAES as storage technology. Figure 5.7a shows a heatmap of the calculated storage capacities for all simulations Figure 5.7b shows a heatmap of the total system cost for all simulations. Table 5.4 shows the values of the simulations that resulted in the lowest and highest storage capacities and total system cost.

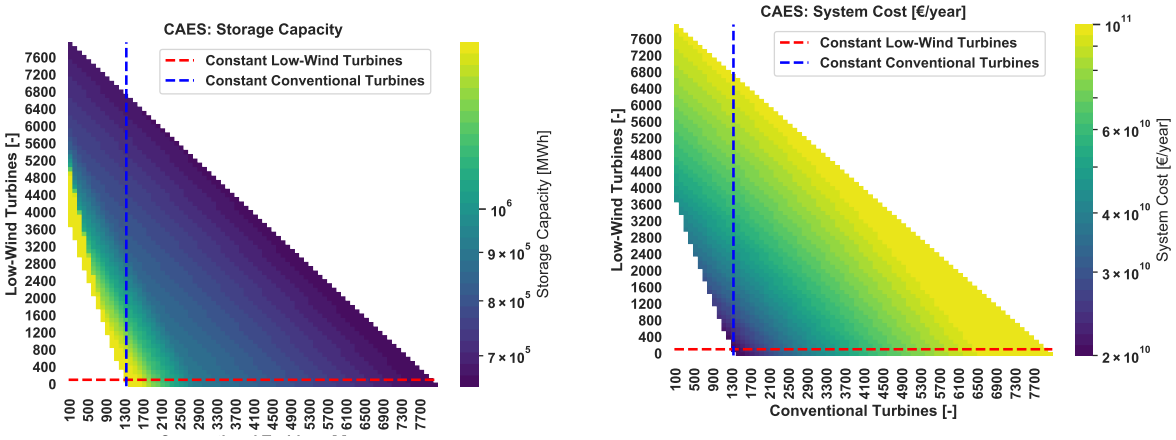

(a) CAES: Storage Capacities for Different Amounts of Conventional and Low-Wind Turbines

(b) CAES: Total System Cost for Different Amounts of Conventional and Low-Wind Turbines

Figure 5.7: CAES: Heatmaps showing storage capacities and total system cost for each simulation

Figure 5.7a and table 5.4 show that again, the lowest storage capacities are achieved on the right diagonal border, which are all simulations with high overplanting factors. Comparing Figures 5.5a and 5.7a side by side, it can be seen that they are identical. This is confirmed when comparing the simulations for the lowest and highest storage capacity, tabulated in Tables 5.3 and 5.4. This result can be explained by the fact that these storage technologies are modelled with the same parameters for efficiency and depth of discharge. The main difference between CAES and the other storage technologies is the fact that the cost of this technology is a function of its maximum needed power, instead of its capacity. As a result the storage costs for CAES are slightly lower than for VRFB. Again, wind costs dominate the system costs, resulting in the simulation with minimal costs now occurring at 1300 conventional and 100 Low-Wind turbines. This simulation has the minimal amount of turbines required to satisfy all constraints. The simulation with 1400 conventional turbines has a fractionally higher cost of 1.886×10^{10} €/yr, due to higher wind costs. The storage costs for both simulations are identical, meaning they were based on the same required maximum power output. From this information, it can be concluded that in this case Low-Wind turbines have a minimal effect on minimising

Table 5.4: Minimum and Maximum values for all simulations using CAES Storage technology

	Unit	Minimum Storage Capacity	Minimum System Cost	Maximum Storage Capacity	Maximum System Cost
Conventional Turbines	turbines	8000	1300	100	8000
Lowwind Turbines	turbines	0	100	3700	0
Overplanting Factor	-	5.20	1.12	1.09	5.20
Storage Capacity	10^6 MW h	0.65	2.477	7.92	0.666
Import	MW h	1452	1588	3549	1452
Export	10^6 MW h	39.862	0.8756	0	39.862
Wind Cost	10^{10} €/yr	12.01	1.880	4.5415	12.01
Storage Cost	10^{10} €/yr	0.0181	0.00529	0.00528	0.0181
System Cost	10^{10} €/yr	12.01	1.885	4.5421	12.01

storage capacity. Again, the chosen turbine step size between simulations plays an important role in the outcome of the minimal cost simulations. If a step size of a single turbine were chosen, the minimum cost simulation would probably contain between 1300 and 1399 conventional turbines, and between 0 and 100 Low-Wind turbines, with a maximum combined amount of 1400 turbines.

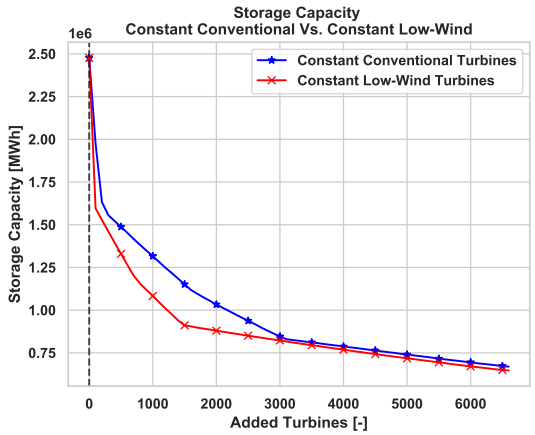

(a) CAES: Storage Capacity Graphs for Constant Conventional and Constant Low-Wind Turbines

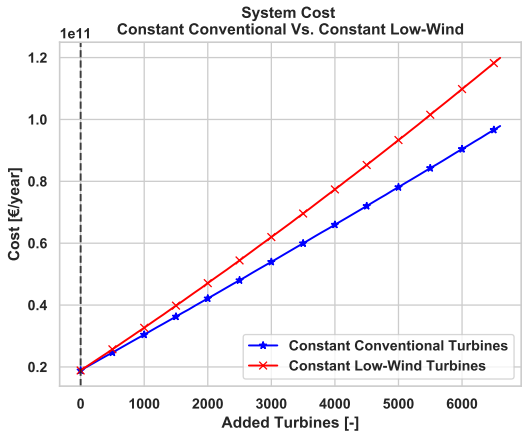

(b) CAES: System Cost Graphs for Constant Conventional and Constant Low-Wind Turbines

Figure 5.8: CAES: Cross-sections through heatmaps, showing trends in storage capacity and system cost for constant conventional and constant Low-Wind turbines

Figures 5.8a and 5.8b show the horizontal and vertical cross-section through the simulation with minimal system cost. Since the minimum cost solution lies on the border of the heatmap, subtracting turbines is not possible. The storage capacity lines shown here are different from those for VRFB, as the cross-section now occurs at 100 Low-Wind turbines, instead of 0. Figure 5.8a shows that, when close to the minimum system cost, adding turbines to the system has a significant effect on the storage capacity. From 0 to around 200 added turbines, the effect on reducing storage capacity is comparable. From 200 to 3000 the line for constant Low-Wind turbines is lower, meaning that adding conventional turbines has a greater effect on the reduction of storage capacity than Low-Wind turbines. After about 3000 turbines both turbines have a similar effect on storage capacity again. Figure 5.8b shows that adding conventional turbines is more expensive than adding Low-Wind turbines.

From the information provided by the storage capacity heatmap, it can be concluded that Low-Wind turbines do not contribute to the minimisation of storage capacity, since the simulation with minimum storage capacity does not contain Low-Wind turbines. The system costs heatmap shows that Low-Wind turbines minimally contribute to minimising total system costs, since the minimum cost simulation

contains a small amount Low-Wind turbines. However, this is an effect of the fact that wind costs dominate the total system costs. Moreover, this can be an effect of the chosen step size.

When looking at the horizontal and vertical cross-sections, it can be concluded that Low-Wind turbines can provide a cost-effective alternative for reducing the total storage capacity in some situations. Conventional turbines have a greater effect on the reduction of storage capacity, but at greater costs. In the situation where the storage capacity at minimum system costs is not feasible, more wind generation has to be installed to lower this capacity. In that case, Low-Wind turbines could provide a cost-effective alternative to conventional turbines. Identical to the simulations with VRFB, wind costs dominate the systems cost, and therefore the simulation with minimal costs appears at the bottom left corner of the heatmap, where the least amount of turbines are installed.

5.2.4. Lithium-Ion Batteries

This section presents the outcome of the model, when using Lithium-ion batteries as storage technology. Figure 5.9a shows a heatmap of the calculated storage capacities for each simulation. Figure 5.9b shows a heatmap of the total system cost for each simulation. Table 5.5 shows the simulations and respective outputs that resulted in the minimum and maximum storage capacity an system costs.

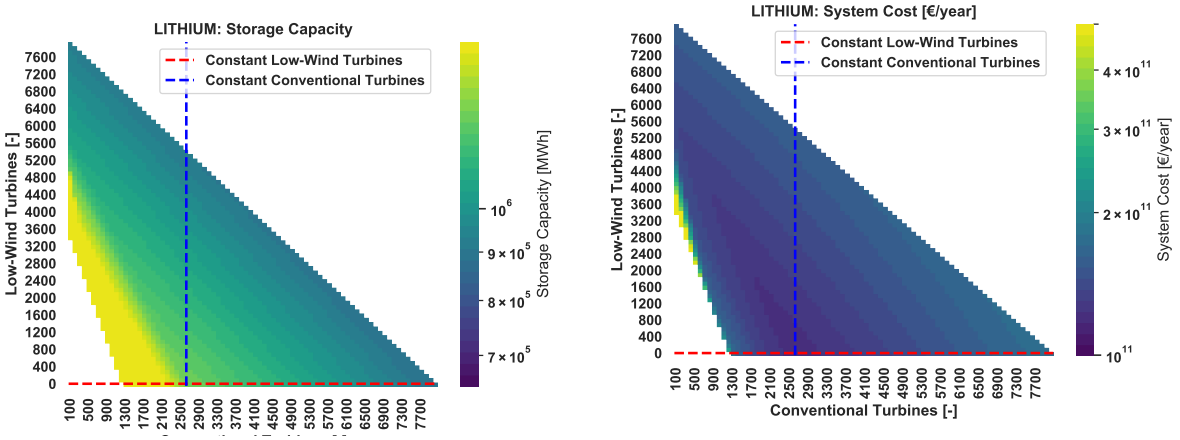

(a) Lithium: Storage Capacities for Different Amounts of Conventional and Low-Wind Turbines

(b) Lithium: Total System Cost for Different Amounts of Conventional and Low-Wind Turbines

Figure 5.9: Lithium: Heatmaps showing storage capacities and total system cost for each simulation using Lithium as a storage technology

Table 5.5: Minimum and Maximum values for all simulations using Lithium Storage technology

	Unit	Minimum Storage Capacity	Minimum System Cost	Maximum Storage Capacity	Maximum System Cost
Conventional Turbines	turbines	8000	2600	100	100
Lowwind Turbines	turbines	0	0	3400	3400
Overplanting Factor	-	5.20	1.90	1.03	1.03
Storage Capacity	10^6 MW h	0.883	1.2763	12.83	12.83
Import	MW h	1452	1225	3186	3186
Export	10^6 MW h	40.11	27.41	0	0
Wind Cost	10^{10} €/yr	12.01	3.55	4.16	4.16
Storage Cost	10^{10} €/yr	0.577	8.33	83.81	83.81
System Cost	10^{10} €/yr	17.77	11.88	87.97	87.97

Figure 5.9a shows the lowest storage capacities on the right diagonal border, which are all simulations with high overplanting factors. The simulation with the lowest storage capacity occurs at 8000 conventional turbines and 0 Low-Wind turbines, which is the same as for VRFB and CAES. This further strengthens

the conclusion that Low-Wind turbines do not contribute to minimising storage capacity. Comparing Figure 5.9a with Figures 5.5a and 5.7a, it can be seen that for lithium, storage capacities are higher compared to VRFB and CAES. This result can be explained by the fact that the maximum depth-of-discharge (DoD) for lithium is lower, at 80 %. Because of this reduced DoD, Lithium requires a larger capacity in order to be able to store enough energy. Figure 5.9b now shows a global minimum system cost along the bottom border of the system cost heatmap, at 2600 conventional and 0 Low-Wind turbines. It can be seen that the range of system costs, indicated by the color bar of the heatmap, is an order of magnitude higher than for VRFB and CAES. The higher system costs are a result of several factors: higher price per kW h, shorter lifespan and higher storage capacities due to limited DoD and yearly degradation of the available storage capacity. The combined effect of all these factors results in significantly higher storage costs, which are now in the same order of magnitude as wind costs. It can also be seen that for the simulation with minimum cost, storage costs are now higher than wind costs. The effect of this increased storage cost is that the minimum cost simulation has moved towards increasing the amount of turbines and thereby the overplanting factor. It can also be seen that for these model parameters, Low-Wind turbines do not contribute to the minimisation of storage costs.

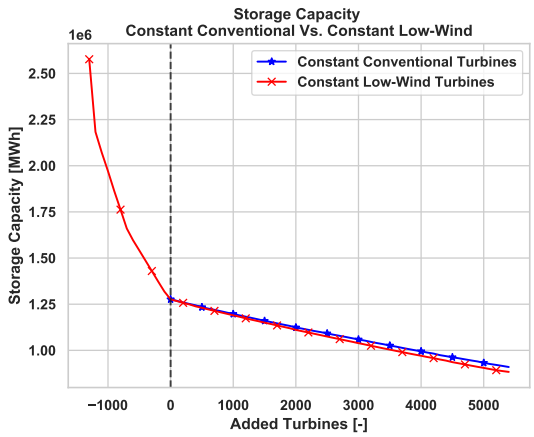

(a) Lithium: Storage capacity graphs for constant conventional and constant Low-Wind turbines

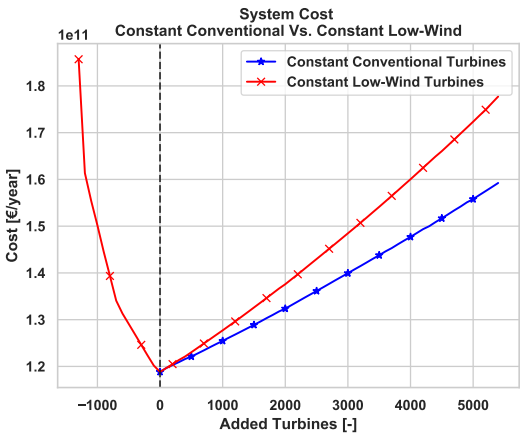

(b) Lithium: System cost graphs for constant conventional and constant Low-Wind turbines

Figure 5.10: Lithium: Cross-sections through heatmaps, showing trends in storage capacity and system cost for constant conventional and constant Low-Wind turbines

Figures 5.10a and 5.10b show the horizontal and vertical cross-section of the heatmap, through the simulation with minimal system costs. Since this simulation lies on the bottom border of the heatmap, only conventional turbines can be subtracted. Figure 5.10a shows that between 0 and around −1300 turbines, the storage capacity shows an exponential increase for subtraction of conventional turbines. Because of the low overplanting in this region of the heatmap, the amplitude and frequency of the mismatch increases, putting a large strain on the storage. The high cost of storage in these model settings means that the minimum cost solution now consists of a trade-off between overplanting and installing extra storage capacity. The lines between 0 and 5400 added turbines show that both conventional and Low-Wind turbines have a similar effect on the reduction of required storage capacity. Figure 5.10a shows that, when looking at the minimum, subtraction of conventional turbines leads to an exponential increase in costs. This is the result of the exponential increase in required storage capacity. It can also be seen that adding conventional turbines increases the system costs more rapidly than adding conventional turbines. Since the effect of both turbines on storage reduction is similar, it can be said that Low-Wind turbines provide a cost-effective alternative in the situation where the minimum cost storage capacity is not feasible.

From the information provided by the storage capacity heatmap, it can be concluded that Low-Wind turbines do not contribute to the minimisation of storage capacity, since the simulation with minimum storage cost does not contain Low-Wind turbines. The system costs heatmap shows that Low-Wind turbines also do not contribute to minimising total system costs, since the minimum cost simulation does not contain Low-Wind turbines. As the wind costs for all simulations are constant between VRFB, CAES

and Lithium, this result can be explained by the increased storage capacity needed for Lithium. For each combination of conventional and Low-Wind turbines, more storage capacity is needed for Lithium than for VRFB and CAES. This increased storage capacity, combined with its increased specific cost, degradation and short lifespan, results in the storage costs being in the same order of magnitude as wind costs. The end result of this is that the simulation with optimal costs consists of a trade-off between storage costs and wind costs.

5.3. Sensitivity Analysis

This section presents and discusses the results of the sensitivity analysis. The goal of the sensitivity analysis is to assess the consequences of the choices in this study on the outcome and to generalise the results, so broader conclusions can be drawn about the effects of Low-Wind and storage costs. The parameters that are assessed in the sensitivity analysis are the CAPEX of the Low-Wind turbines and the CAPEX and OPEX of the different storage technologies. The selected parameters within the model are varied using a cost factor. The cost factors scale the desired parameter up or down, after which the total system cost is recalculated, and the minimum cost simulation is found. When a variation of a certain parameter results in drastically different results, this means that the value of this parameter has to be set accurately and requires careful consideration. On the other hand, when a variation in a parameter does not result in significantly different results, the accuracy of this parameter is not deemed very important for the final result.

5.3.1. Low-Wind CAPEX

This section presents and discusses the results of the sensitivity analysis on the CAPEX of the Low-Wind turbine. The Low-Wind CAPEX is varied, but the OPEX is kept constant, to make sure we only see the effect of the Low-Wind turbine scaling and cost model. The Low-Wind CAPEX cost factors is varied between 0 en 4, with 0.1 increments. The OPEX of the Low-Wind turbines is not varied, as a large share of the turbine OPEX comes from logistic and equipment that do not differ between Low-Wind and conventional turbines. The results of the sensitivity analysis on the Low-Wind turbine CAPEX are shown in Figure 5.11. For each storage technology, the trend lines show the shifting of the simulation with minimum costs on the overplanting heatmap, as shown in Figure 5.4. Next to each heatmap a 2D representation of the respective trend line is shown, in order to show the direction of the trend line for increasing cost factors. With this information it can be assessed whether variation of a certain parameter has a significant impact on the results. The markers on the lines represent an integer cost factor. The same process is repeated and shown for the sensitivity analysis of storage CAPEX and OPEX.

For VRFB, at cost factors of 0.8 and lower, the simulation with minimum total costs moves to the simulations with 1300 conventional and 100 Low-Wind turbines. In this cost factor region the reduction of wind costs, achieved by the lower cost of Low-Wind turbines, outweighs the increased storage cost. For cost factors higher than 0.8 the simulation stays at the original simulation with 1400 conventional turbines.

For CAES, at cost factors of 1 and lower, the simulation with minimum system costs stays at the original simulation of 1300 conventional and 100 Low-Wind turbines. In this cost factor region the reduction of wind costs, achieved by the lower cost of Low-Wind turbines, outweighs the increased storage cost. For higher cost factors the reduction this is no longer true and it switches to the simulation with 1400 conventional turbines. After this point, further increasing of the Low-Wind CAPEX seems to have no effect on the results.

For Lithium, only at a cost factor of 0 is there movement of the minimum cost simulation. At this cost factor, the minimum cost simulation moves to the simulation with 1500 conventional and 1900 Low-wind turbines. However, This cost factor is not considered a valid result, since Low-Wind turbines can not be built and installed for zero cost. For all other cost factors the simulation stays at the original simulation of 2600 conventional turbines.

From this information several conclusions can be drawn. For both VRFB and CAES, the model shows similar behaviour. In both cases the location of the minimum cost solutions shows very low

sensitivity to the CAPEX of the Low-Wind turbine. For small Low-Wind cost factors, the wind cost reduction achieved by exchanging 100 conventional for Low-Wind turbines outweighs the increase in storage cost. For these model settings, wind costs dominate the system costs and as a result the minimum cost simulation aims to minimise the amount of wind turbines. In both situations the optimal solution lies in the region of low overplanting.

In the case of Lithium, where storage costs and wind costs appear in the same order of magnitude, the minimum cost simulation shows no movement for a change in Low-Wind costs. Only for zero Low-Wind CAPEX does the simulation move, but since Low-Wind turbines can not be built and installed for free, this is not considered a valid result. Reducing the CAPEX of the Low-Wind turbines essentially reduces the slope in the vertical direction of the system cost heatmap. However, the installed Low-Wind turbines still have to be maintained and operated, incurring OPEX. Increasing or decreasing the slope does not result in movement of the simulation with minimum costs.

For situations where wind costs dominate system costs, the model is not sensitive to the cost of the Low-Wind turbine. When the optimum situation already does not contain Low-Wind turbines, increasing the cost will obviously not shift the optimum towards Low-Wind turbines. The reduction of the Low-Wind turbine CAPEX also has very little effect on the simulation. For situation where storage and wind cost are in the same order of magnitude and the minimum cost simulation contains no Low-Wind turbines, the model is also not sensitive to the CAPEX of the Low-Wind turbine. This result can be explained by the fact that the installation of Low-Wind turbines still incurs OPEX, while being less effective at reducing storage capacity than conventional turbines. Even increasing the Low-Wind CAPEX to near-zero does not make them cost-competitive with conventional turbines, in this case.

5.3.2. Storage CAPEX & OPEX

This section presents and discusses the results of the sensitivity analysis on the cost of the storage technologies. For this analysis, both the storage CAPEX and OPEX are varied. This is done, because for all storage technologies the OPEX is calculated as a percentage of the CAPEX. The OPEX of the storage components is assumed to be largely dominated by replacement cost of parts rather than logistics and equipments, as opposed to the OPEX of the Low-Wind turbine. Hence, changing the CAPEX automatically also changes the OPEX. The cost factor for the storage solution is varied between 0 and 5 for VRFB and CAES, and between 0 and 20 For CAES and Lithium, 0.1 increments. For Lithium the storage cost factor range is varied over a larger range in order to show the entire movement of the trend line. The large range of cost factors is not meant to show the effect of the uncertainty of Lithium storage cost, but rather is meant to generalise the results. This way the conclusion that are drawn can be applied to different storage technologies which have similar technical parameters as Lithium, but cover this large range of specific costs. Figure 5.12 presents the results of the sensitivity analysis on the storage CAPEX and OPEX. The markers on the lines represent an integer cost factor.

For VRFB, the model only shows movement of the minimum cost simulation for very low storage cost factors, between 0 and 0.2. for storage cost factors between 0 and below 0.2, the minimum cost simulation lies at the simulation with 1300 conventionial and 100 Low-Wind turbines. In this cost factor region, wind cost purely dominate the system cost and the model aims to minimise the installed turbine capacity. Again, in this cost factor region the cost reduction achieved by installing 100 Low-Wind turbines in stead of conventional, outweighs the increased storage cost. for storage cost factors of 0.2 and higher, the minimum cost simulation lies at the simulation with 1400 conventional turbines. In this cost factor region, the cost reduction achieved by the Low-Wind turbines no longer outweighs the increased storage costs, and therefore the simulation moves towards the other simulation with the lowest feasible amount of turbines, which also has a lower storage capacity.

For CAES, the model shows no movement of the minimum cost simulation for changing storage costs. For these settings, wind cost purely dominate the total system costs and the model aims to minimise the cost of installed turbine capacity.

For Lithium, the model shows movement of the minimum cost simulation for the entire range of storage cost factors. For storage cost factors between 0 and 1, the minimum cost simulation moves from the left diagonal border and trends towards regions with higher overplanting. In this cost factor region, the cost of storage becomes increasingly dominant, and therefore the simulation with minimum

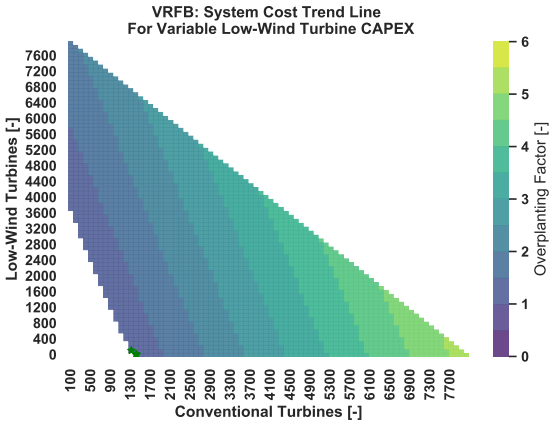

(a) VRFB: Location of minimum cost simulation for changing Low-Wind turbine CAPEX

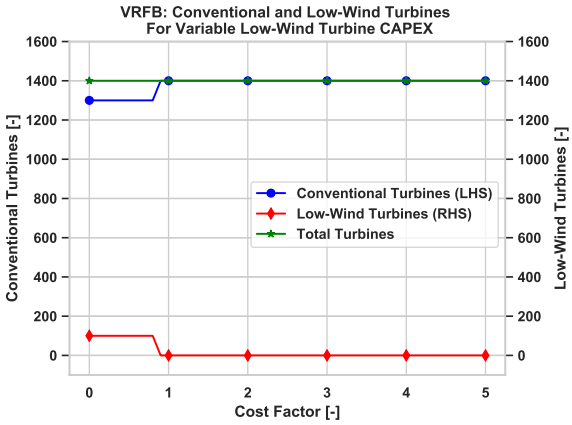

(b) VRFB: offshore turbine composition of minimum cost simulation for changing Low-Wind turbine CAPEX

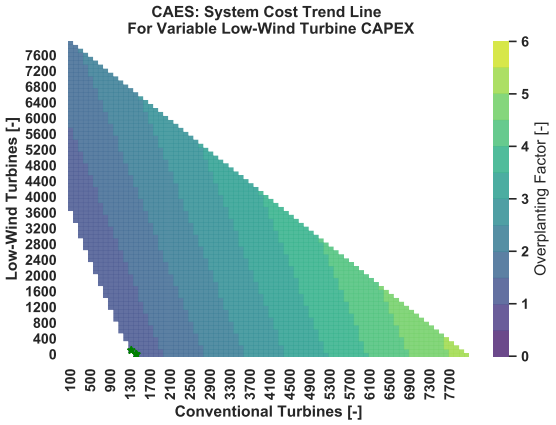

(c) CAES: Location of minimum cost simulation for changing Low-Wind turbine CAPEX

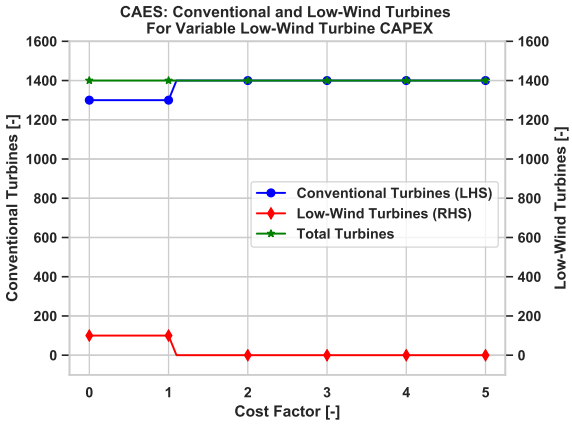

(d) CAES: offshore turbine composition of minimum cost simulation for changing Low-Wind turbine CAPEX

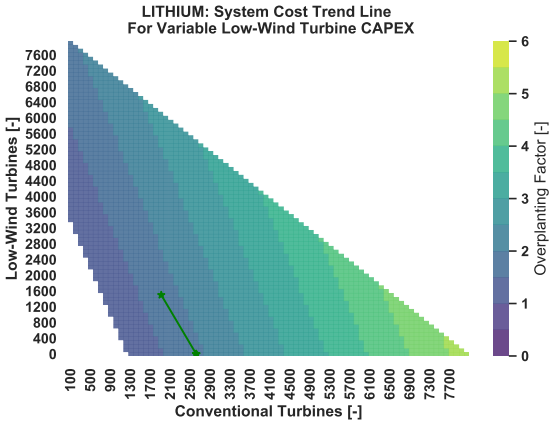

(e) Lithium: Location of minimum cost simulation for changing Low-Wind turbine CAPEX

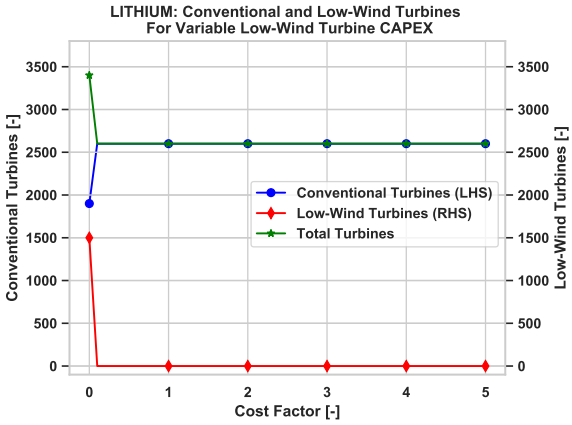

(f) Lithium: offshore turbine composition of minimum cost simulation for changing Low-Wind turbine CAPEX

Figure 5.11: Results of sensitivity analysis performed on the Low-Wind Turbines CAPEX for the different storage technologies

cost consists of a trade-off between wind costs and storage costs. Therefore the minimum system cost simulation trends towards installing more turbines. In this cost factor region, the Low-Wind turbines do not contribute to the simulation with minimum costs. For storage cost factors between 1 and 2.6, the model shows a high sensitivity to storage costs. In this cost factor region the minimum cost simulation lies within the heatmap. Here, three things can be seen happening. First, the minimum cost simulation

trends towards increasing total installed turbine capacity, which can be seen by the upward slope of the green line in Figure 5.12f. This indicates that for increasing storage costs, the minimum cost solution trends towards overplanting and reducing storage capacity. Secondly, Low-Wind turbines increasingly contribute to the minimum cost simulation. This contribution peaks at a cost factor of around 2.5. Thirdly, although installed total capacity and installed Low-Wind both increase, the amount of overproduction stays largely constant. The fact that, for a certain range of cost factors, the overplanting factor stays relatively constant means that their effect is not a result of increasing the yearly produced energy, but rather that of reducing the occurence and amplitude of the mismatch during moments of low wind speeds. Since conventional and Low-Wind turbines essentially behave the same at low wind speeds, but Low-Wind turbines are less expensive, they become cost-effective. This shows that, for a certain range of storage costs, Low-Wind turbines can provide a cost-effective solution to minimising system cost. From Section 5.2.4 we know that at a cost factor of 1 the largest share of the total system cost comes from storage costs. For higher cost factors, this share only increases. For storage cost factors of 2.6 and higher, the model shows a high sensitivity to storage costs. In this cost factor region, the system cost become increasingly dominated by storage costs. Low-Wind turbines decreasingly contribute to the simulation with minimum system cost, since conventional turbines are more effective at reducing the required storage capacity. For increasing storage costs, the model favors a higher ration of conventional turbines.

When looking at the overal shape of the trendline along the heatmap, it can be seen that this line crosses the minimum cost solution that were found in the initial simulations. It can be said that this trendline represent the entire spectrum of system costs options, ranging from dominated purely by wind costs to dominated largely by storage costs. For very low storage cost factors, where storage costs dominate the system cost, the simulation also lies in the bottom left corner. Then, for moderate storage costs overplanting becomes important, but Low-Wind turbines do not yet contribute in the minimum cost solution. For high storage cost factors, storage costs become increasingly dominant, and the Low-Wind turbine becomes a cost-effective solution for the minimisation of system cost. For very high cost factors the model aims to minimise storage capacity, and the minimum cost simulation trends to even larger overplanting factors by saturating the available area. Since in this situation the available space is limited, and conventional turbines are more effective at reducing storage capacity than Low-Wind turbines, the share of conventional turbines increases for increasing storage cost factors.

From the information above, The following conclusions can be drawn. In a system where the costs are dominated by wind costs, the objective becomes to minimise the amount of wind turbines. In these cases, Low-Wind turbines do not contribute to a reduction of total system cost. In a system where the costs are dominated by storage costs, the minimum cost simulation aims to minimise the storage capacity by overplanting winid turbines. This is mainly achieved by fully saturating all the available offshore wind farm area available with wind turbines. However, in these systems where storage costs dominate, the Low-Wind turbines seem to be able to provide a cost-effective solution to minimising total system cost.

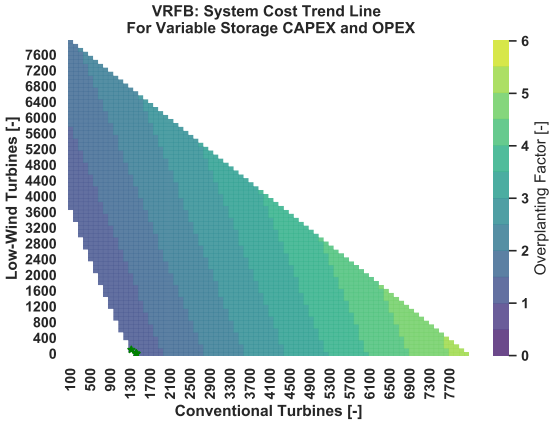

(a) VRFB: location of minimum cost simulation for changing storage CAPEX and OPEX

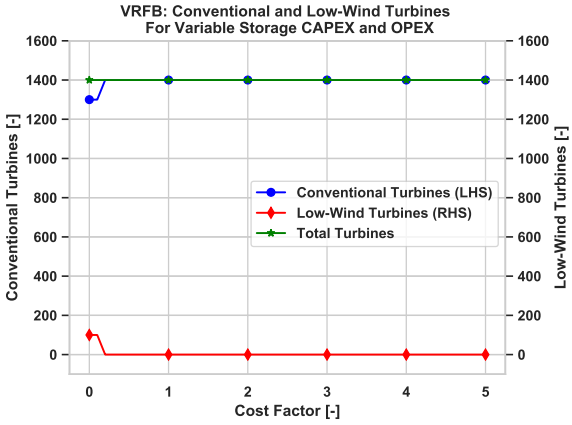

(b) VRFB: offshore turbine composition of minimum cost simulation for changing storage CAPEX and OPEX

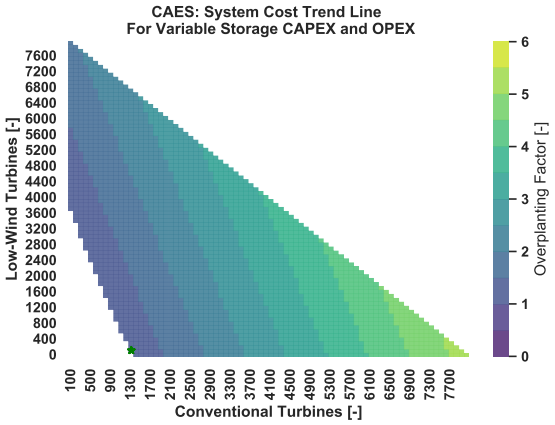

(c) CAES: location of minimum cost simulation for changing storage CAPEX and OPEX

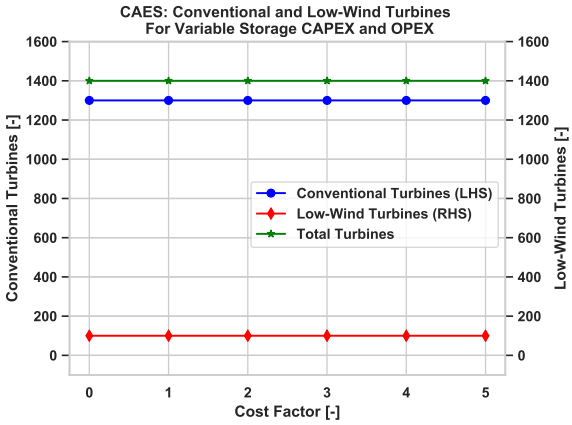

(d) CAES: offshore turbine composition of minimum cost simulation for changing storage CAPEX and OPEX

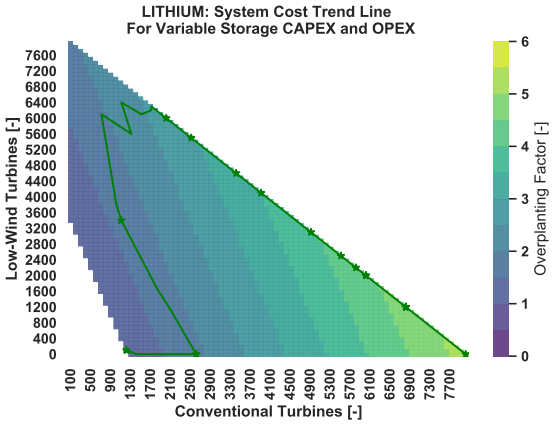

(e) Lithium: location of minimum cost simulation for changing storage CAPEX and OPEX

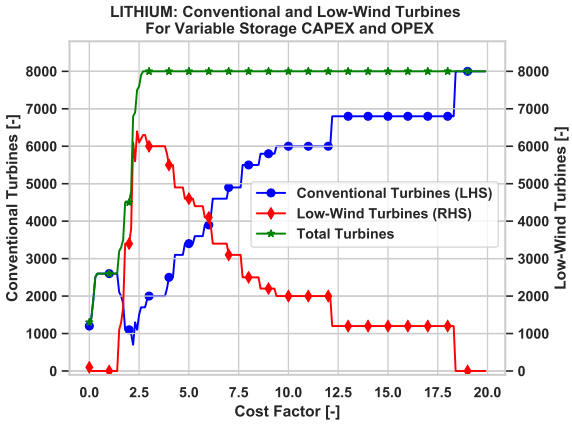

(f) Lithium: offshore turbine composition of minimum cost simulation for changing storage CAPEX and OPEX

Figure 5.12: Results of sensitivity analysis performed on the different storage technologies CAPEX and OPEX

6

Conclusion

This chapter concludes the work done in this thesis. In this chapter the research questions, stated in Section 1.4, are answered. The research methods are reflected upon and the general conclusion that can be drawn from the results are presented.

6.1. Key Findings

This thesis assessed the effectiveness of the Low-Wind turbine concept on the reduction of required large scale seasonal storage and costs, within the Dutch power system. In order to complete this assessment, several sub-questions have been posed to help structure and divide the different components that were needed in order to answer the final question. In the sections below, VRFB and CAES are considered the low-cost storage technologies, while Lithium is considere to be the high-cost storage technology.

6.1.1. What will be the cost of a Low-Wind turbine?

The Low-Wind turbine design resulted in a 26 % cost reduction compared to the conventional turbine with equal rotor swept area, but higher rated power. This result was achieved by the redesign of the IEA 15 MW Reference turbine into a 4.33 MW Low-Wind turbine.

However, the chosen modelling approach for the support structure resulted in an unwanted positive gradient in tower diameter and wall thickness, which requires attention when moving further with the design. Also, a check of the natural frequency of the new support structure shows possible interference with the average wave period of the North Sea. The cost of the generator of the Low-Wind turbine is solely based on its rated power, which might not be accurate for the large range over which the rated power has been scaled. Ultimately, it can be concluded that the Low-Wind turbine design was largely successful, since the main goal was to determine a reasonable cost figure for this turbine.

6.1.2. What is the effect of implementing Low-Wind turbines in the Dutch power system on the required seasonal storage capacity?

The results show that Low-Wind turbines are less effective at the reduction of the required seasonal storage capacity than conventional multi-MW turbines. For all storage technologies assessed in this study, the lowest storage capacity was needed when all available offshore wind farm space was filled with conventional wind turbines.

According to the results, overplanting is the most effective solution for reducing the required storage capacity, and adding conventional turbines increases overplanting more rapidly then Low-Wind turbines. When a simulation has low overplanting, mismatch occurs more frequently and their respective amplitudes are higher. Therefore, the system requires large storage capacities in order to deal with these moments. In turn, increasing overplanting reduces the occurrence of mismatch and reduces their respective amplitude. This in turn reduces the amount of energy that needs to be stored within the seasonal storage, and reduces its required rated power.

When the required storage capacity to obtain the most cost-effective system can not be achieved, adding conventional turbines is more effective at reducing storage capacity than Low-Wind turbines.

For low-cost storage technologies, wind costs dominate the system costs. In these cases the most cost-effective system requires large storage capacities and adding conventional turbines is more effective at increasing overplanting and thereby reducing storage capacity. Only for high overplanting factors do they show similar results. When more expensive storage technologies are required in the system, larger overplanting factors become increasingly cost-effective. In these cases the addition of both conventional and Low-Wind turbines may have similar effectiveness in further reduction of the required storage capacity.

6.1.3. What is the effect of different storage technologies on the required seasonal storage capacity?

The results of the different storage technologies showed that the efficiency, depth of discharge (DoD)and lifetime of the storage technology have an effect on the required storage capacity. The results of VRFB and CAES show no difference in required storage capacity. This can be explained by the fact that they have the same characteristics for efficiency and DoD. The results of Lithium showed higher storage capacities are higher compared to VRFB and CAES, mainly due to it reduced DoD and lifetime.

6.1.4. What is the effect of implementing Low-Wind turbines in the Dutch power system on the system costs?

When using low-cost storage technologies, Low-Wind turbines show little to no effect on the cost of the power system. In these situations, wind costs dominate the system cost and therefore wind costs are minimised by installing as little storage capacity as possible.

When using storage technologies with higher costs, Low-Wind turbines show no effect on the cost of the power system. In this case, the most cost-effective solution lies in a region with higher overplanting, but Low-Wind turbines are not installed in the minimum cost simulation.

In general, it can be concluded that Low-Wind turbines do not directly contribute to the minimum system costs. However, at high overplanting factors their effect on storage capacity is similar to conventional turbines, and they achieve this result at lower costs. Therefore, in situations where the storage capacity required for minimum costs can not be achieved and high overplanting is required, Low-Wind turbines may be able to provide a cost-effective solution.

6.1.5. What is the effect of different storage technologies on the system costs?

The results with the low-cost storage technologies show that their costs can be considered negligible compared to wind costs. Because of this, the most cost-effective simulation has large storage capacities and low overplanting. The results also show little difference between calculation of storage costs based on required capacity or required rated power. For high-cost storage technologies, the results show that storage costs become an increasingly dominant components of the system costs. The higher cost can be caused by higher specific cost, shorter lifespan or a combination of the two.

6.1.6. how sensitive are the results to the cost of the Low-Wind turbines?

The sensitivity analysis performed on the CAPEX of the Low-Wind turbine shows little effect on the location of the minimum cost simulation for all storage technologies.

For low-cost storage technologies, for certain Low-Wind turbine CAPEX, the minimum cost simulation contains Low-Wind turbines. This effect goes away for increased Low-Wind CAPEX. The switch between the two simulations happens at the Low-Wind cost factor where the cost reduction achieved by the Low-Wind turbines equals the extra cost incurred from the increased storage capacity.

For high-cost storage technologies, only when Low-Wind CAPEX is reduced to zero does the simulation switch to a simulation which contains Low-Wind turbines.

In general, the sensitivity analysis showed that,for these model settings, the model is not sensitive to Low-Wind turbine costs. This sensitivity analysis further proved that Low-Wind turbines minimally contribute to the minimum cost solution, even when their CAPEX is set to zero. Because Low-Wind turbines are less effective at reaching the desired yearly demand, many of them need to be installed. The extra OPEX that results from this increased amount makes them an unfavourable option.

6.1.7. How sensitive are the results to the cost of the storage technologies?

For the low-cost storage technologies, the sensitivity analysis performed on the storage CAPEX and OPEX showed little effect on the location of the minimum cost simulation. For very low storage cost factors, the cost reduction achieved by installing Low-Wind turbines outweighs the cost of the increased storage capacity. This essentially is the same behaviour as shown in the sensitivity analysis performed on the Low-Wind turbine CAPEX. For increasing cost factors the model showed no sensitivity.

For the high-cost storage technologies, the sensitivity analysis essentially showed the entire spectrum of cost dominance possibilities, ranging from dominated by wind costs to dominated by storage costs. Because of this, more general conclusions can be drawn about the effectiveness of Low-Wind turbines. It again proved that for situations where wind costs dominate, the minimum cost simulation aims to reduce the amount of installed turbines, and in those cases Low-Wind turbines do not contribute to this simulation. When storage costs become increasingly dominant, the minimum cost simulation trends towards overplanting. In this situation, the Low-Wind turbines still do not provide a cost-effective alternative. However, when storage cost become even higher, both conventional and Low-Wind turbines show a similar effect on the reduction of storage capacity, while Low-Wind turbines can do this at lower cost. In this situation, Low-Wind turbines can be a cost-effective solution to minimising system cost. When all available offshore wind farms are fully saturated and storage cost is increased even higher, the minimum cost simulation trends towards higher overplanting. Since conventional turbines do this more effectively, the cost-effectiveness of Low-Wind decreases until all wind farms only contain conventional turbines.

6.2. Recommendations

Several recommendations for research topics that can further deepen the knowledge about the effectiveness of the Low-Wind turbine are stated below:

- The study can be repeated using meteorological and demand data of a different year or country, in order to see if the same conclusions can be drawn. It might be the case that the particular datasets used in this study are not representative of an average year, and therefore give skewed results.
- The effectiveness of Low-Wind turbines on other services within the energy market, such as frequency containment, can be investigated.
- The effect of a more diverse mix of turbines can be investigated. In reality the portfolio of installed wind turbines is much more diverse than just three turbines. This mix of different turbines might alter the effectiveness of the Low-Wind turbines.

Bibliography

Amelang, Sören (2018). *Renewables cover about 100% of German power use for first time ever | Clean Energy Wire*. URL: https://www.cleanenergywire.org/news/renewables-cover-about-100-german-power-use-first-time-ever (visited on 08/13/2021).

Amelang, Sören et al. (Jan. 2018). *The causes and effects of negative power prices | Clean Energy Wire*. URL: https://www.cleanenergywire.org/factsheets/why-power-prices-turn-negative (visited on 08/13/2021).

Ardelean, Mircea. et al. (2015). *HVDC submarine power cables in the world : state-of-the-art knowledge.* Tech. rep. European Commision, p. 78.

Baxter, Richard (2019). "2018 Energy Storage Pricing Survey." In: December. URL: https://www.osti.gov/servlets/purl/1592892.

Bortolotti, P. et al. (2019). "A detailed wind turbine blade cost model". In: *Nrel* June, pp. 1–69.

Bortolotti, Pietro et al. (2019). "Systems Engineering in Wind Energy - WP2.1 Reference Wind Turbines". In: *IEA Wind TCP Task 37* May. URL: https://www.osti.gov/biblio/1529216-iea-wind-tcp-task-systems-engineering-wind-energy-wp2-reference-wind-turbines.

BVG Associates (2019). "A Guide to an Offshore Wind Farm Updated and extended". In: *Publ. behalf Crown Estate Offshore Renew. Energy Catapult* January, pp. 1–70. ISSN: 1751-4223. URL: http://www.thecrownestate.co.uk/guide%7B%5C_%7Dto%7B%5C_%7Doffshore%7B%5C_%7Dwindfarm.pdf.

Canet, Helena et al. (2020). "On the scaling of wind turbine rotors". In: *Wind Energy Sci. Discuss.* March, pp. 1–35. ISSN: 2366-7443. DOI: 10.5194/wes-2020-66.

CBS (2021). *StatLine - Aardgas en elektriciteit, gemiddelde prijzen van eindverbruikers*. URL: https://opendata.cbs.nl/statline/%7B%5C#%7D/CBS/nl/dataset/81309NED/table?ts=1625403229587%7B%5C&%7Dfromstatweb=true (visited on 07/04/2021).

Dalla Riva, Alberto et al. (2017). "IEA Wind TCP Task 26: Impacts of Wind Turbine Technology on the System Value of Wind in Europe". In: November, p. 101.

Ecosmartsun (2021). *PV System Performance: GHI to PoA - EcoSmart™ Solar*. URL: https://ecosmartsun.com/pv-system-performance-3/pv-system-performance-ghi-to-poa/ (visited on 04/27/2021).

ENTSO-E (2021). *ENTSO-E Transparancy platform*. URL: https://transparency.entsoe.eu/load-domain/r2/totalLoadR2/show?name=%7B%5C&%7DdefaultValue=false%7B%5C&%7DviewType=TABLE%7B%5C&%7DareaType=BZN%7B%5C&%7Datch=false%7B%5C&%7DdateTime.dateTime=11.03.2021+00:00%7B%5C%%7D7CCET%7B%5C%%7D7CDAY%7B%5C&%7DbiddingZone.values=CTY%7B%5C%%7D7C10YNL----------L!BZN%7B%5C%%7D7C10YNL----------L%7B%5C&%7DdateTime.timezon (visited on 03/11/2021).

Exchangerates.org.uk (2021). *Euro to US Dollar Spot Exchange Rates for 2020*. URL: https://www.exchangerates.org.uk/EUR-USD-spot-exchange-rates-history-2020.html (visited on 03/08/2021).

Fingersh, L et al. (2006). "Wind Turbine Design Cost and Scaling Model". In: *Nrel* 29.December, pp. 1–43. DOI: 10.1016/j.advwatres.2006.01.003.

Gaertner, Evan et al. (2020a). *Definition of the IEA 15 MW Offshore Reference Wind Turbine*. Tech. rep. International Energy Agency. URL: https://www.nrel.gov/docs/fy20osti/75698.pdf.

— (2020b). *IEA-15-240-RWT/Documentation at master · IEAWindTask37/IEA-15-240-RWT*. URL: https://github.com/IEAWindTask37/IEA-15-240-RWT/tree/master/Documentation (visited on 03/30/2021).

— (2021). *IEA-15-240-RWT/WT_Ontology at master · IEAWindTask37/IEA-15-240-RWT*. URL: https://github.com/IEAWindTask37/IEA-15-240-RWT/tree/master/WT%7B%5C_%7DOntology (visited on 04/02/2021).

General Electric (2021). *World's Most Powerful Offshore Wind Platform: Haliade-X | GE Renewable Energy*. URL: https://www.ge.com/renewableenergy/wind-energy/offshore-wind/haliade-x-offshore-turbine (visited on 07/16/2021).

Harlan, Léon et al. (1996). *Stepped tower memo.pdf*.

Hersbach, H. et al. (2018). *ERA5 hourly data on single levels from 1979 to present. Copernicus Climate Change Service (C3S) Climate Data Store (CDS)*. DOI: 10.24381/cds.adbb2d47. URL: https://cds.climate.copernicus.eu/cdsapp%7B%5C#%7D!/dataset/reanalysis-era5-single-levels?tab=overview (visited on 04/08/2021).

IPCC (2021). *Summary for Policymakers. In: Climate Change 2021: The Physical Science Basis. Contribution of Working Group I to the Sixth Assessment Report of the Intergovernmental Panel on Climate Change*. Tech. rep. 3-4. IPCC, pp. 433–440. URL: https://www.ipcc.ch/report/ar6/wg1/downloads/report/IPCC%7B%5C_%7DAR6%7B%5C_%7DWGI%7B%5C_%7DSPM.pdf.

Keegan, M. H. et al. (2013). "On erosion issues associated with the leading edge of wind turbine blades". In: *J. Phys. D. Appl. Phys.* 46.38. ISSN: 00223727. DOI: 10.1088/0022-3727/46/38/383001.

Komusanac, Ivan et al. (2020). *Wind energy in Europe in 2019*. Tech. rep. WindEurope. URL: https://windeurope.org/wp-content/uploads/files/about-wind/statistics/WindEurope-Annual-Statistics-2019.pdf.

Laboratories, Sandia National (2021). *PV Performance Modeling Collaborative CEC Inverter Test Protocol*. URL: https://pvpmc.sandia.gov/modeling-steps/dc-to-ac-conversion/cec-inverter-test-protocol/ (visited on 04/29/2021).

Lavidas, George et al. (2019). "North sea wave database (NSWD) and the need for reliable resource data: A 38 year database for metocean and wave energy assessments". In: *Atmosphere (Basel)*. 10.9, pp. 1–27. ISSN: 20734433. DOI: 10.3390/atmos10090551.

Madsen, Helge Aagaard et al. (2019). "The LowWind turbine concept for optimal system integration Outline". In.

Manwell, J.F. et al. (2002). *Wind Energy Explained*. Amherst: John Wiley & Sons Ltd., p. 590. ISBN: 0470846127.

May, Nils (2017). "The impact of wind power support schemes on technology choices". In: *Energy Econ.* 65, pp. 343–354. ISSN: 01409883. DOI: 10.1016/j.eneco.2017.05.017. URL: http://dx.doi.org/10.1016/j.eneco.2017.05.017.

Ministerie van Economische zaken en Klimaat (2019). "Klimaatakkoord". In: *Klimaatakkoord*, p. 250. URL: https://www.klimaatakkoord.nl/binaries/klimaatakkoord/documenten/publicaties/2019/06/28/klimaatakkoord/klimaatakkoord.pdf.

NREL (2019a). *3. Drivetrain Components — WISDEM 2.0 documentation*. URL: https://wisdem.readthedocs.io/en/latest/wisdem/drivetrainse/components.html (visited on 03/08/2021).

— (2019b). *Theory — WISDEM 2.0 documentation*. URL: https://wisdem.readthedocs.io/en/latest/wisdem/nrelcsm/theory.html (visited on 03/08/2021).

— (2020). *WISDEM/WISDEM: Wind Plant Integrated System Design and Engineering Model*. URL: https://github.com/WISDEM/WISDEM.

Renewable Energy World (2021). *Demystifying LCOE | Renewable Energy World*. URL: https://www.renewableenergyworld.com/solar/demystifying-lcoe/%7B%5C#%7Dgref (visited on 07/02/2021).

Rijksdienst voor Ondernemend Nederland (2020). *Monitor Wind op Land 2019*. Tech. rep. Rijksdienst Voor Ondernemend Nederland. URL: https://www.rijksoverheid.nl/documenten/rapporten/2020/06/26/bijlage-monitor-wind-op-land-2019.

Royal Haskoning DHV (2017). *Offshore Wind Dogger Bank*. Tech. rep. Royal Haskoning DHV, p. 11. URL: https://northseawindpowerhub.eu/wp-content/uploads/2017/10/Wind-Capacity-Study.pdf.

Smets, Arno H M et al. (2016). *Solar Energy*. UIT, p. 484. ISBN: 978-1-906860-32-5.

SPARTA (2021). *SPARTA - Portfolio Review 2018/19*. URL: http://fr.zone-secure.net/-/Sparta%7B%5C_%7DPortfolio%7B%5C_%7DReview%7B%5C_%7D2018%7B%5C_%7D2019/-/?%7B%5C_%7D%7B%5C_%7Dhstc=20425319.023c5d84b3d34f421c5a307e7e8e612f.1580910940466.1580910940466.1580910940466.1%7B%5C&%7D%7B%5C_%7D%7B%5C_%7Dhssc=20425319.1.1580910940467%7B%5C&%7D%7B%5C_%7D%7B%5C_%7Dhsfp=3480816081%7B%5C&%7DhsCtaTracking=fc42f905-7ce3-4212-baf2-1480855e8 (visited on 04/14/2021).

Tamrakar, Ujjwol et al. (2017). “Virtual inertia: Current trends and future directions”. In: *Appl. Sci.* 7.7. ISSN: 20763417. DOI: 10.3390/app7070654.

Ulbig, Andreas et al. (2014). *Impact of low rotational inertia on power system stability and operation*. Vol. 19. 3. IFAC, pp. 7290–7297. ISBN: 9783902823625. DOI: 10.3182/20140824-6-za-1003.02615. arXiv: 1312.6435. URL: http://dx.doi.org/10.3182/20140824-6-ZA-1003.02615.

UNESCO (2021). *Dutch EEZ Map*. URL: http://msp.ioc-unesco.org/wp-content/uploads/2016/02/Netherlands%7B%5C_%7Dsmall.jpg (visited on 05/04/2021).

Westegg (2021). *The Inflation Calculator*. URL: https://westegg.com/inflation/ (visited on 03/08/2021).

Wikipedia (2021). *Windturbines in Nederland - Wikipedia*. URL: https://nl.wikipedia.org/wiki/Windturbines%7B%5C_%7Din%7B%5C_%7DNederland (visited on 05/04/2021).

Zaayer, Michiel et al. (2018). “Introduction to wind turbines: physics and technology”. In: p. 160.

Zaayer, Michiel B. (2000). “Starting-point and Methodology of Cost Optimisation for the Conceptual Design of DOWEC .” In.